Determining Carrier Mobilities

in GaAs and Natural Pyrite

Using Geometrical Magnetoresistance Measurement

by

Aditya Ravi

A Thesis Presented in Partial Fulfillment
of the Requirements for the Degree
Masters of Science

Approved April 2016 by the
Graduate Supervisory Committee:

Nathan Newman, Chair
Rakesh Singh
David K Ferry

ARIZONA STATE UNIVERSITY

May 2016

ABSTRACT

Measurements of the geometrical magnetoresistance of a conventional semiconductor, gallium arsenide (GaAs), and a more recently developed semiconductor, iron pyrite (FeS_2) were measured in the Corbino disc geometry as a function of magnetic field to determine the carrier mobility (μ_m). These results were compared with measurements of the Hall mobility (μ_H) made in the Van der Pauw configuration. The scattering coefficient (ξ), defined as the ratio between magnetoresistance and Hall mobility (μ_m/μ_H), was determined experimentally for GaAs and natural pyrite from 300 K to 4.2 K. The effect of contact resistance and heating on the measurement accuracy is discussed.

i

ACKNOWLEDGEMENT

TABLE OF CONTENTS

LIST OF TABLES

LIST OF FIGURES

INTRODUCTION

Iron pyrite has recently received a lot of attention for use in photovoltaic cells because of its high abundance, 0.95 eV band gap [1, 2] non-toxicity and very high absorption coefficient (10^5 cm^{-1} for energies >1.4 eV). The high absorption coefficient results in a 0.1 μm thick layers being able to absorb over 90% of the sunlight light in that spectral region. This can be compared to >200 μm for silicon [3]. The many advantages of this material has inspired a number of studies aimed at synthesizing pyrite thin films and quantum dots using advanced growth techniques including Metal Organic Chemical Vapor Deposition (MOCVD)[4], Sputtering[5], Molecular Beam Epitaxy (MBE) Physical Vapor Evaporation (PVD),Sol-gel and nano ink deposition.[6]

Despite the strong effort in producing thin films, pyrite photovoltaic cells have only been able to yield cell efficiencies <3% and open circuit voltages of only ~0.1 V [3], From this, we can conclude that efforts to develop practical applications using pyrite semiconductors have not been successful.[2-7]

In a recent study conducted by our research group, Vahidi et al [7] were able to produce single phase thin films that were epitaxial on natural pyrite substrates and polycrystalline on Si and SiO$_2$ surfaces.

Carrier conduction and doping mechanism in pyrite thin films and bulk materials are not yet well understood. In the majority of cases, bulk crystals are n-type and thin films are p-type conduction. The root cause of these observations is not understood. The role of the surface in affecting the nature of transport has been in debate for many years [8, 9]. One factor that plays a role is that the films produced to date are mostly high defective with small mobilities (<3 cm^2 \V·s) [2-9].

MOBILITY

In a solid, carriers drift at a velocity that is proportional to the applied electric field v=μE, where the constant of proportionality is called the mobility. The unit for mobility is $m^2/(V.s)$ in the SI system and is $cm^2/(V.s)$ in the CGS system. They are related by 1 $m^2/(V.s)$ =10^4 $cm^2/(V.s)$

The main factors determining the mobility are effective mass of the carriers (m^*) and the scattering time (τ), as expressed in the equation

$$\mu = \frac{e\tau}{m^*}$$ (1.1)

The scattering time is defined as the time from when the carriers are first ballistically accelerated by the electric field until they are scattered by a phonon or impurity. The microscopic scattering depends on the nature of the scatterer, the carrier trajectory in relation to the scatterer and the energy of the carrier.

Conductivity is proportional to the product of mobility and the carrier concentration as given by the relation

$$\sigma = (nq\mu_e + pq\mu_h)$$ (1.2)

where 'n' is the electron concentration in cm^{-3}, 'p' is the hole concentration in cm^{-3}, 'μ_e' is the electron mobility in $cm^2/(V.s)$, 'μ_h' is the hole mobility in $cm^2/(V.s)$ and 'q' is the charge of an electron given 1.6 x 10^{-19} C.

TRANSPORT IN SEMICONDUCTORS

In equilibrium, semiconductor carriers are distributed among the energy levels given by Fermi-Dirac statistics

$$f(E) = \frac{1}{1+e^{\frac{(E-E_f)}{KT}}}$$ (1.3)

where E is the energy of the energy level, E_f is the energy at the fermi level, K is the Boltzmann constant and T is the temperature. Under the equilibrium condition no net transport of charge or energy occurs. When an external force or temperature gradient

is applied, the carriers will not remain in equilibrium, as first explained by Ludwig Boltzmann in 1872 [10]. He proposed an equation now known as the Boltzmann transport equation

$$\frac{df}{dt} = \frac{1}{\hbar} F_t . \nabla_k f + v . \nabla_r f + \frac{\partial f}{\partial t} \qquad (1.4)$$

On the right side of equation (1.4) the first term takes into account changes in distribution due to forces on the carrier, the second term accounts for changes due to concentration gradients in the carrier distribution and the last term represents the local time dependent change in the distribution function.

When the semiconductor material is subjected to a electric field 'E' and a magnetic field 'B', the charge carriers experience a force 'qE+v x B', this is called the Lorentz force. Retaining the temperature and concentration gradient, under the relaxation time assumption, the function $'f'$ is replaced by the term $\frac{f-f_0}{\tau_m}$, where f_0 is the equilibrium distribution given by Fermi Dirac function given in equation 1.3. Applying this condition in equation (1.4) we get

$$\frac{f-f_0}{\tau_m} = \frac{q}{\hbar}(E + v \, X \, B).\nabla_k f - v.\nabla_r f \qquad (1.5)$$

From the above equation, when we consider drift velocity V_d as the average velocity of the carriers over the distribution and when we introduce dimensionless variables we get

$$v_d = \frac{-qE}{m^*} < \tau_m > \qquad (1.6)$$

where E is the Electric field applied. In the above equation, the proportionality constant between drift velocity and the electric field is the conductivity mobility, μ_c. Thus equation (1.6) can be expressed as

$$v_d = \mu_c E \qquad (1.7)$$

The momentum relaxation time has a simple power dependence on energy of the form

$$\tau_m = \tau_0 \left(\frac{\varepsilon}{K_B T}\right)^r \tag{1.8}$$

In the above equation 'r' has different values depending on the type of scattering mechanism.

Solving eq. (1.5) for current density 'j' we get

$$J = \frac{q^2 n}{m^*}\left\langle\frac{\tau_m}{1+(\omega_c\tau_m)^2}\right\rangle - \frac{q^3 n}{m^{*2}}\left\langle\frac{\tau_m^2}{1+(\omega_c\tau_m)^2}\right\rangle(E \times B) + \frac{q^4 n}{m^{*3}}\left\langle\frac{\tau_m^3}{1+(\omega_c\tau_m)^2}\right\rangle B(E.B) \tag{1.9}$$

where ω_c is the cyclotron frequency

$$\omega_c = \frac{q|B|}{m^*} \tag{1.10}$$

The first term in eq. (1.9) is the ohmic term. The factor $1+(\omega_c\tau_m)^2$ in the denominator is responsible for the magnetoresistance term. The second term results in the Hall effect term, which also includes a magnetoresistance term associated with it. The third term is an additional second order magnetoresistance factor [11].

<div style="text-align:center">HALL EFFECT</div>

In the year 1879 Edwin Hall discovered that when a solid is sourced with current 'I$_s$' and is kept in a magnetic field 'B' perpendicular to the applied electric field, the charge carriers experience a Lorentzian force (-qV X B) perpendicular to the direction of the sourced current and the applied magnetic field (see fig 1). In the steady state, there is an electric-field generated perpendicular to the current flow. The transverse voltage produced on the corresponding surfaces is called the Hall voltage (V_H)[12].

$$V_H = \frac{I_S B}{qnt} \tag{1.11}$$

where 'I$_s$' is the sourced current, 'B' is the magnetic field, 'E' is the electric field, 't' is the sample thickness, 'V' is the particle velocity, 'n' is the a charge carrier density and 'q' is the charge of the electron (1.602 x 10^{-19} C).

If the Hall voltage is negative then the majority charge carriers are electrons and the material is n-type, while if the Hall voltage is positive then the majority carriers are holes and the material is p-type.
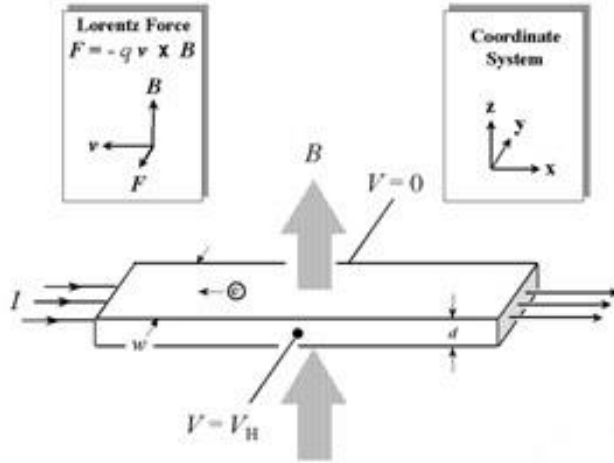
Figure 1: Hall effect on a semiconductor of thickness 'd', I is the current sourced, B is the magnetic field acting perpendicular to the plane of the sample, V$_H$ is the Hall Voltage generated

In the Hall measurements, the carrier concentration can be inferred from the following relationship

$$n = \frac{I_s \times B}{(q \times V_H \times t)} \tag{1.12}$$

By using the Van der Pauw configuration as described in the next section we can determine the sheet resistance (R$_s$) through which one can infer Hall mobility from:

$$\mu_H = \frac{|V_H|}{R_s * I_s * B} \tag{1.13}$$

The resistivity 'ρ' can be determined using the sheet resistance R$_s$ by the relation $\rho = R_s t$, where 't' is the material's thickness.

RESISTIVITY MEASUREMENTS

A four point Van der Pauw configuration was used to measure both Hall voltage and resistivity of the sample. With this method it is preferred to use one of following measurement configurations that are shown below. In our experiments, we use the configuration 'b' on a square sample
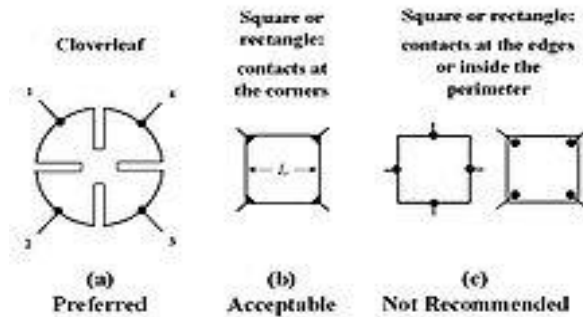
Figure 2: Different Van der Pauw configurations, for our Hall and resistivity measurements, we have used the configuration (b) [13]

The contacts on the semiconductor should be made such that the average diameter of the contacts, d and the thickness of the sample, t, should be smaller than the distance between the contacts, L. Relative errors caused by finite sized contacts is of the order of d/L

To perform the Hall and magnetoresistance measurements, the following equipment is required:

• An instrument that generates magnetic field.

• Constant-current source.

• High input impedance nano-voltmeter.

• Sample temperature-measuring probe

In our case we will use a commercial cryostat (Quantum Design, Model Physical Property Measurement System (PPMS)) for generating the required magnetic fields and controlling the temperature.

6

SAMPLE CONFIGURATION FOR MEASURING RESISTIVITY

To perform resistivity measurements in the Van der Pauw configuration, four leads were connected to the four ohmic contacts on the sample. These are labeled 1, 2, 3, and 4 as shown in fig.3. It is important to use the same type of contacts and wires for all four leads in order to minimize thermoelectric effects.

We define the following parameters:

ρ = sample resistivity (in $\Omega \cdot cm$)

d= conducting layer thickness (in cm)

I_{12}= positive dc current I sourced into contact 1 and taken out of contact 2. Likewise for I_{23}, I_{34}, I_{41}, I_{21}, I_{14}, I_{43}, I_{32} (in amperes, A)

V_{12} = dc voltage measured between contacts 1 and 2 (V_1-V_2) without applied magnetic field (B= 0). Likewise for V_{23}, V_{34}, V_{41}, V_{21}, V_{14}, V_{43}, V_{32} (in volts, V)
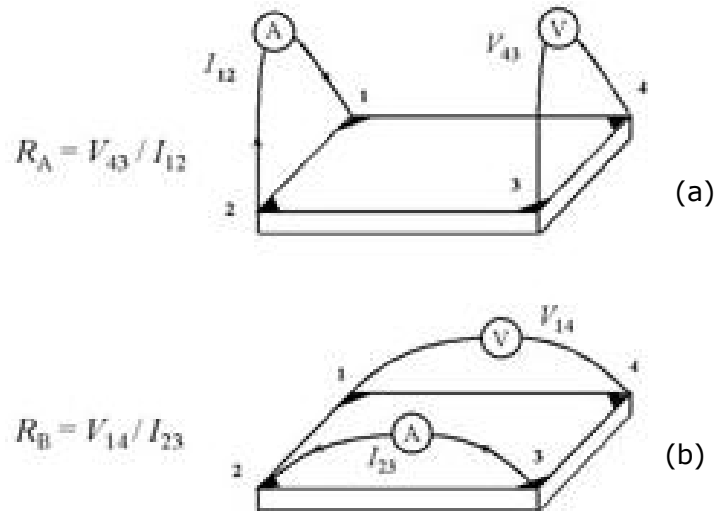
Figure 3: Van der Pauw measurement schematic, (a) shows R_A is the resistance in vertical direction (b) shows R_B is the resistance in horizontal direction[14]

PROCEDURE TO MEASURE RESISTIVITY

- A dc current 'I' is applied to the sample that is set to a value high enough to obtain a measureable low-noise signal, while being small enough to prevent significant heating. This current value and measurement sequence was controlled using the LABVIEW program

- Apply current I_{21} and measure voltage V_{34}

- Polarity of the current was reversed (I_{12}) and measure V_{43}

- This was repeated for the remaining six values (V_{41}, V_{14}, V_{12}, V_{21}, V_{23}, V_{32})

Eight measurements of voltage yield the following eight values of resistance

$$R_{21,34} = V_{34}/I_{21}, \; R_{12,43} = V_{43}/I_{12}, \tag{1.14}$$

$$R_{32,41} = V_{41}/I_{32}, \; R_{23,14} = V_{14}/I_{23},$$

$$R_{43,12} = V_{12}/I_{43}, \; R_{34,21} = V_{21}/I_{34},$$

$$R_{14,23} = V_{23}/I_{14}, \; R_{41,32} = V_{32}/I_{41}.$$

Important consistency checks on measurement repeatability, ohmic contact quality, and sample uniformity were done. If any of the above equality conditions were off by greater than 5 % (preferably 3 %), the measurements were considered invalid and the source of the error was investigated.

$$R_{21,34} = R_{12,43} \qquad\qquad R_{43,12} = R_{34,21} \tag{1.15}$$

$$R_{32,41} = R_{23,14} \qquad\qquad R_{14,23} = R_{41,32}$$

$$R_{21,34} + R_{12,43} = R_{43,12} + R_{34,21} \text{ and} \tag{1.16}$$

$$R_{32,41} + R_{23,14} = R_{14,23} + R_{41,32}.$$

RESISTIVITY CALCULATIONS

The sheet resistance R_S was determined from the two characteristic resistances, R_A which is the resistance along the vertical direction and R_B being the resistance along the horizontal direction.

$$R_A = (R_{21,34} + R_{12,43} + R_{43,12} + R_{34,21})/4 \tag{1.17}$$

$$R_B = (R_{32,41} + R_{23,14} + R_{14,23} + R_{41,32})/4$$

The Van der Pauw equation for a square sample with ohmic contacts on the corners of the sample is given by the relation

$$e^{\left(-\frac{\pi * R_A}{R_s}\right)} + e^{\left(-\frac{\pi * R_B}{R_s}\right)} = 1 \tag{1.18}$$

By substituting R_A and R_B in the above equation, we can infer the sheet resistance R_S. If the conducting layer thickness 't' is known, the bulk resistivity $(\rho = R_s * t)$ can then be calculated from R_S.

HALL MEASUREMENTS

Two sets of Hall measurements, one for positive and one for negative magnetic field direction were taken. The relevant definitions are as follows

- I_{13} = dc current sourced into lead 1 and taken out of lead 3. Likewise for I_{31}, I_{42}, and I_{24}.

- B = constant and uniform magnetic field intensity (to within 3 %) applied perpendicular to the direction of the current source as shown in fig.4. B is positive when pointing out of plane of the sample, and negative when pointing into the plane of the sample

- V_{24P} = Hall voltage measured between leads 2 and 4 with magnetic field positive for I_{13}. Likewise for V_{42P}, V_{13P}, and V_{31P}. Similar definitions for V_{24N}, V_{42N}, V_{13N}, and V_{31N} apply when the magnetic field B is reversed.

PROCEDURE FOR MEASURING HALL EFFECT

The procedure for the Hall measurement was:

- Apply a positive magnetic field B

- Apply a current I_{13} to leads 1 and 3 and measure V_{24P}

- Apply a current I_{31} to leads 3 and 1 and measure V_{42P}

- Likewise, measure V_{13P} and V_{31P} with I_{42} and I_{24}, respectively

- Reverse the magnetic field (negative B)

- Likewise, measure V_{24N}, V_{42N}, V_{13N} and V_{31N} with I_{13}, I_{31}, I_{42}, and I_{24}, respectively

Table 1: 8-Hall voltages measured

Magnetic Field direction	Hall Voltage measured
Positive field (B+)	V_{24P}
	V_{42P}
	V_{13P}
	V_{31P}
Negative field(B-)	V_{24N}
	V_{42N}
	V_{13N}
	V_{31N}

The above 8 measurements of Hall voltages V_{24P}, V_{42P}, V_{13P}, V_{31P}, V_{24N}, V_{42N}, V_{13N}, and V_{31N} determine the sample type (n or p) and the carrier concentration 'n'. The Hall mobility can be determined from the carrier concentration 'n' and the sheet resistance 'R_S' obtained in the resistivity measurement. See Eq. (1.18).

The Hall voltage from each of the two diagonal sets of contacts can be averaged to obtain improved accuracy.
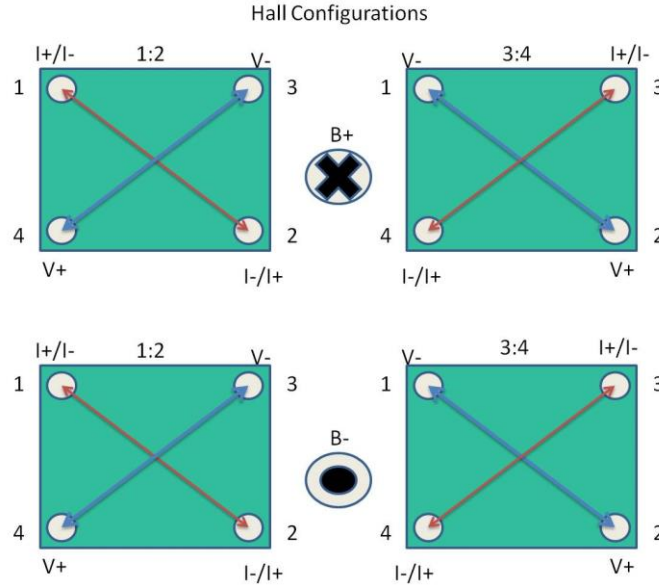
Figure 4: Schematic configuration used for measuring 8 Hall voltages, Red arrows indicate the direction of source current and the blue arrows indicate the corresponding Hall voltage measurement.

HALL CALCULATIONS

The following steps have been used to determine the carrier density and Hall mobility:

- For a given current source, four Hall Voltages have been obtained by subtracting measured Hall voltages taken in the negative and positive magnetic field direction.

$$V_C = V_{24P} - V_{24N}, V_D = V_{42P} - V_{42N}, \quad (1.19)$$

$$V_E = V_{13P} - V_{13N}, \text{ and } V_F = V_{31P} - V_{31N}.$$

- We average the obtained four Hall voltages to determine the mean value (V_H) and standard deviation(σ) and check the validity by ensuring that the values fall within 5%.

- The sample type is determined from the polarity of the voltage V_H. If the Hall voltages are positive (negative), the sample is p-type (n-type).

11

- The sheet carrier concentration (in units of cm^{-3}) is calculated from

$$P= \frac{10^{-8}*IB}{[qV_H t]}, \text{ if the voltage sum is positive, or} \qquad (1.20)$$

$$n=\frac{10^{-8}*IB}{[qV_H t]}, \text{ if the voltage sum is negative,}$$

where B is the magnetic field in gauss (G) and I is the dc current in amperes (A).

- The Hall mobility $\mu = \frac{V_H}{R_s IB}$ (in units of cm^{2}V^{-1}s^{-1})

DISADVANTAGES OF HALL MEASUREMENT TECHNIQUE

As we have shown, by performing Hall and resistivity measurements we can determine the carrier type, carrier concentration and mobility. However, there are some disadvantages and limitations to this technique.

- In a highly defective sample, the scattering times of the carrier is short, and this will result in a relatively small Hall voltages. This can make it difficult to obtain accurate results.

- When the mobility is small, on the order or smaller than 10 cm^2/V·s, the Hall voltage is typically small compared to the voltage offset from misaligned contacts and/or asymmetric samples. This makes accurate measurements challenging, particularly in the presence of typical noise levels.

It would be advantageous to use an alternative method that is able to more accurately and reliably measure low-mobility materials. It would also be desirable to be able to perform these measurements using a 2-point measurement scheme.
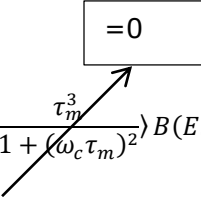
MAGNETORESISTANCE

Magnetoresistance refers to the change in resistance of the conductivity and resistivity as a result of the application of magnetic field.[15]. There are three main types of magnetoresistance, depending on the direction of the magnetic field. If the magnetic field is parallel to the direction of the current sourced it is called longitudinal magnetoresistance. Transverse magnetoresistance effect occurs when the direction of the magnetic field is perpendicular to the current sourced. This again is subdivided into physical magnetoresistance and geometrical magnetoresistance. If the magnetic field is applied at any other direction it is called as anisotropic magnetoresistance. There are other types of magnetoresistance depending on the type of material used like the giant magnetoresistance, colossal magnetoresistance and extraordinary magnetoresistance. In my current work I will be focusing on the geometrical magnetoresistance effect on GaAs and iron pyrite semiconductors.

PRINCIPLE OF GEOMETRICAL MAGNETORESISTANCE

The geometrical magnetoresistance dominates when the current is sourced from one end of a long and narrow sample to the other in a magnetic field applied perpendicular to the sample's long dimension. The equation for magnetoresistance can be derived from eq.1.9, when the magnetic field 'B' is perpendicular to the electric field 'E' [11]:

$$\boxed{=0}$$

$$J = \frac{q^2 n}{m^*} \langle \frac{\tau_m}{1+(\omega_c \tau_m)^2} \rangle - \frac{q^3 n}{m^{*2}} \langle \frac{\tau_m^2}{1+(\omega_c \tau_m)^2} \rangle (E \times B) + \frac{q^4 n}{m^{*3}} \langle \frac{\tau_m^3}{1+(\omega_c \tau_m)^2} \rangle B(E.B)$$

$$J = \frac{q^2 n}{m^*} \langle \frac{\tau_m}{1+(\omega_c \tau_m)^2} \rangle - \frac{q^3 n}{m^{*2}} \langle \frac{\tau_m^2}{1+(\omega_c \tau_m)^2} \rangle (E \times B) \qquad (1.21)$$

From eq. 1.13

$$\omega_c = \frac{q|B|}{m^*}, \text{ and}$$

$$\tau_m = \frac{\mu m^*}{q}$$

Substituting the values of ω_c and τ_m in eq.1.21 and considering small magnetic fields such that $\mu B < 1$ we get

$$\frac{R(B)-R(0)}{R(0)} = \xi(\mu B)^2 + C \qquad (1.22)$$

where R(B) is the resistance of the sample at magnetic field B, R(0) is the resistance of the sample at zero magnetic field, ξ is the scattering coefficient of the sample which is given as the ratio of magnetoresistance and Hall mobility (μ_m/μ_H)[16] and 'C' is the constant arising due to the Hall term

When a sample is used that is not long and narrow, the Hall Voltage is present and can dominate the results. In the following figure 5, we can see the equipotential lines in a bar shaped sample and how Hall effect arises in such samples
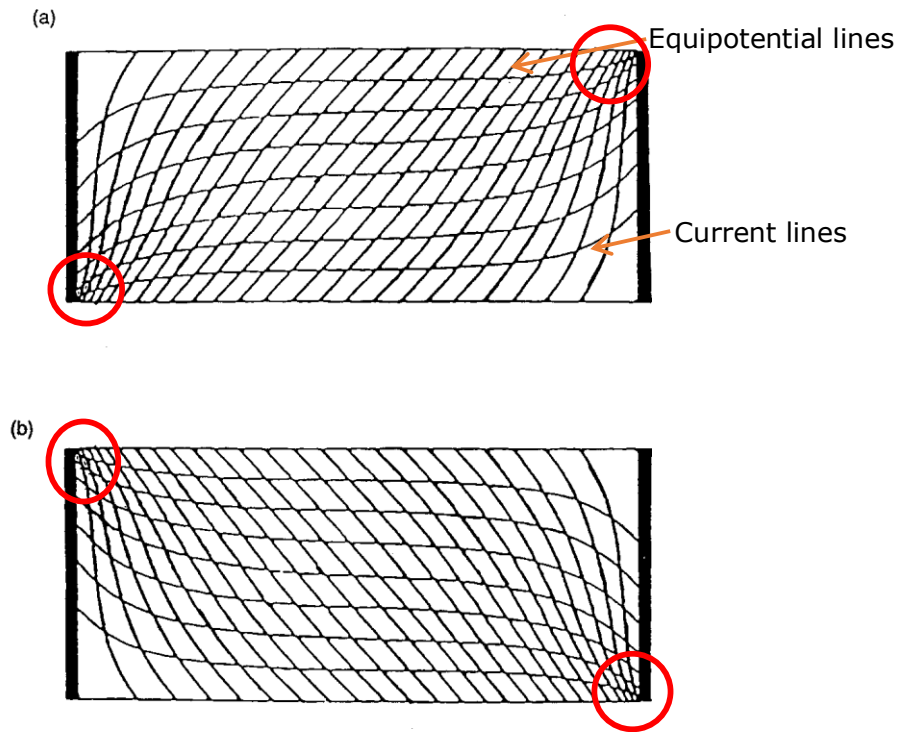
Figure 5: The current and the equipotential lines in a bar shaped sample in a magnetic field perpendicular to the plane of the drawing(a) is out of the plane and (b) is into the plane, the red circles indicate the accumulation of hall voltages on the contacts.[17]

In order to eliminate the errors associated with the Hall Effect on the magnetoresistance, Orso Mario Corbino in the year 1911 described an arrangement of using a cylindrical structure that can negate the effects of charge accumulation due to the Hall effect. In their proposed arrangement the contact consist of a conducting annulus with perfectly conducting rims as shown in fig.6. When the magnetic field is zero, radial current flows between the rims. When the magnetic field is applied perpendicular to the current, a circular current is generated. As the magnetic field is increased, the radial current decreases and the circular component of current increases, which results in an increase in the resistance of the sample [15].Since the change in resistance is observed due to the geometry, it is called the geometric magnetoresistance.

15
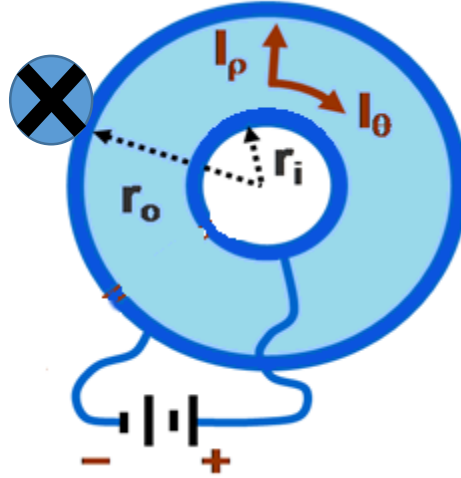
Figure 6: Schematic of Corbino disk configuration for the magnetoresistance measurement with the field perpendicular to the current source

In the case of Corbino disk, the l/w ratio of the contacts is equal to infinity therefore the Hall voltages are effectively shorted out. Under those conditions eq.1.22 becomes

$$\frac{R(B)-R(0)}{R(0)} = \xi(\mu B)^2 \qquad (1.23)$$

where R(B) is the resistance of the sample at magnetic field B, R(0) is the resistance of the sample at zero magnetic field, $'\xi'$ is the scattering coefficient of the sample which is given as the ratio of magnetoresistance and hall mobility (μ_m/μ_H)[16].

MAGNETORESISTANCE MEASUREMENTS

The 2-point magnetoresistance measurement was carried out in the presence of a magnetic field on the Corbino disk samples. Two measurements sets were taken, one for positive and one for negative magnetic field direction. The relevant definitions are as follows

I_S = dc current sourced into inner contact and taken out of outer contact.

B = constant and uniform magnetic field intensity (to within 3 %) applied perpendicular to the direction of the current source as shown in fig. 6. B is positive

16

when pointing outside the plane of the sample, and negative when pointing into the plane of the sample

V_P = Hall voltage measured between inner and outer contact with magnetic field positive for I_S

Similar definitions for V_N apply when the magnetic field B is reversed.

Generally when the contacts are ohmic, the magnetoresistance measurements are symmetric with respect to magnetic field direction and the current source direction, in contrast what we observed in Van der Pauw configuration This illustrated an advantage of using magnetoresistance over Hall for determining mobilities, as the errors due to contact asymmetry are eliminated.

PROCEDURE FOR MEASURING MAGNETORESISTANCE

The procedure for the magnetoresistance measurement was:

- Apply a current 'I_S' to leads and measure 'V'

- Apply a perpendicular magnetic field 'B'

- Apply a current 'I_S' to leads and measure 'V'

- Change the applied magnetic field to desired magnetic with the current source turned on, measure the Voltage

The above measurements Voltages V is used to determine the sample resistance at each and every magnetic field point and use the above equation to determine the mobility of the sample.

MAGNETORESISTANCE CALCULATION

The following steps have been followed to measure the mobility from magnetoresistance

At zero field, $R(0) = V(0)/I_S$

At magnetic field 'B', $R(B) = V(B)/I_S$

$$\frac{\Delta R}{R} = \frac{R(B) - R(0)}{R(0)} \qquad\qquad (1.24)$$

A graph is plotted with $\frac{\Delta R}{R}$ on the abscissa (y axis) and magnetic field squared 'B^2' on the ordinate (x axis). Then the data is fit with a linear equation as $\frac{\Delta R}{R} = aB^2$. The square root of the coefficient of the x term 'a, represents the mobility of the sample.

RESISTANCE OF THE SAMPLE BETWEEN THE CORBINO DISK

To obtain an accurate measurement of the magnetoresistance mobility, it is crucial that a precise value of R, the zero voltage resistance, be determined. Since, the method of measuring magnetoresistance using Corbino Disk sample is a 2-point measurement technique, care must be taken to avoid the effect of contact resistance in the determination of R.

In order to determine an accurate zero field resistance, I chose to use the resistivity of the sample determined by the 4-point van Der Pauw measurements. Then, to infer the resistance in the Corbino geometry, the resistance of the 2-dimensional radial current flow needs to be taken into account. To do this, consider a Corbino disc of inner radius 'r_1' and outer radius 'r_2'(see fig 7), with a small section subtending an angle of dθ with thickness 't' at a point 'dr' from the center of the inner contact
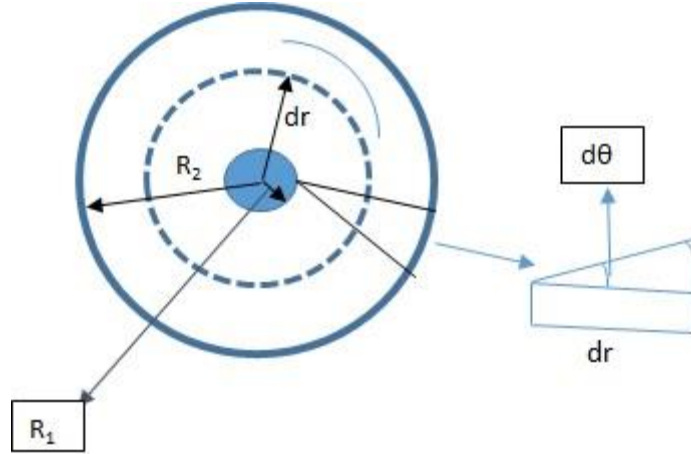
Figure 7: Corbino disk geometry used in our discussion to calculate the resistance of the sample with the inner contact having an OD of R_1 and the outer contact having an ID of R_2.

The area 'A' of the 2D plane between the inner and outer contact is given as

$$A = 2\pi rt$$

The resistance is given as

$$\int_0^R dR = \rho_H \int_{r_1}^{r_2} \frac{dr}{A} = \rho_H \int_{r_1}^{r_2} \frac{dr}{2\pi rt} \qquad (1.25)$$

$$R = \rho_H \left(\frac{\ln(r_2) - \ln(r_1)}{2\pi t} \right)$$

where, $'\rho_H'$ is the resistivity obtained from our Van der Pauw measurements.

ADVANTAGES OF MAGNETORESISTANCE OVER HALL MEASUREMENT

For magnetoresistance measurements, the change in resistance increases quadratically with respect to field, whereas for Hall measurements the Hall voltage scales linearly. Thus, in strongly scattered samples with small Hall mobilities, we can go to high fields to obtain larger signals and improved accuracy. When the magnetoresistance measurement is performed. In such strongly-scattered materials with low mobilities, high field effects, such as cyclotron resonance, will not become significant or affect the results.

ENERGY DEPENDENCE ON SCATTERING TIME AND ITS EFFECT ON MOBILITY

I have described how the mobility depends on the scattering time and the effective mass earlier in the transport chapter. In n-type GaAs, electrons at or near the bottom of the conduction band occupy a single band and have an isotropic effective mass.

When the semiconductor has an isotropic and parabolic energy band, the expression for the scattering time, in the absence of phonon scattering, is given by the relation

$$\tau_m = \tau_0 \left(\frac{x}{K_{B}T}\right)^r \tag{1.7}$$

where x is the electron kinetic energy given by

$$x = E - E_c \tag{1.26}$$

where E is carrier energy, E_C is the energy of conduction band edge.

τ_0 is the carrier lifetime and the exponent 'r' is independent of energy and depends on the type of scattering[11].

The Boltzmann transport equation can be expressed using three fundamental parameters: the Hall mobility, the MR mobility and the effective drift mobility[18].

$$
\left.
\begin{aligned}
\mu_{eff} &= \frac{e}{m^*} \frac{\int_0^\infty E N(E) \tau_m(E) \left(-\frac{\partial f}{\partial E}\right) dE}{\int_0^\infty N(E) f(E) dE} \\[2em]
\mu_{Hall} &= \frac{e}{m^*} \frac{\int_0^\infty E N(E) \tau_m(E)^2 \left(-\frac{\partial f}{\partial E}\right) dE}{\int_0^\infty N(E) f(E) \tau_m(E) \left(-\frac{\partial f}{\partial E}\right) dE} \\[2em]
\text{and} \\[1em]
\mu_{MR} &= \frac{e}{m^*} \sqrt{\frac{\int_0^\infty E N(E) \tau_m(E)^3 \left(-\frac{\partial f}{\partial E}\right) dE}{\int_0^\infty N(E) f(E) \tau_m(E) \left(-\frac{\partial f}{\partial E}\right) dE}}
\end{aligned}
\right\} \tag{1.27}
$$

where f(E) is the Fermi–Dirac distribution function, N(E) the density of states, $\tau_m(E)$ the energy-dependent momentum relaxation time, e the electron charge, and m* the electron effective mass.

From the above equation we can see that

$\mu_{MR} > \mu_{Hall} > \mu_{eff}$

μ_{Hall} is related to the drift velocity given by the relation [19]

$$\mu_{Hall} = r_H \mu_{eff} \tag{1.28}$$

r_H is the Hall Factor

And μ_{MR} is related to the drift mobility μ_{eff} by the relation

$$\mu_{MR} = r_{MR} \mu_{eff} \tag{1.29}$$

r_{MR} is the magnetoresistance factor

The scattering coefficient $'\xi'$ is given as

$$\xi = \frac{r_{MR}}{r_H} \tag{1.30}$$

The values of the Hall and Magnetoresistance mobilities depends on film thickness, doping densities, impurities, strain and effective dimensions in the case of devices[20].

Considering, μ_{eff} to be constant for a particular material the scattering factor can also be determined using the Hall and the magnetoresistance mobility and it is given as

$$\xi = \frac{\mu_{MR}}{\mu_{Hall}} \tag{1.31}$$

EXPERIMENTAL METHODS

SAMPLE PREPERATION

n-type GALLIUM ARSENIDE (GaAs, n-type)

Hall and magnetoresistance studies were performed on n-type GaAs samples with three different doping concentrations. The measured transport parameters as well as those provided by the manufacturers are summarized in the Table 1 below. The reason n-type Gallium Arsenide was chosen to test the validity and reliability of our measurements is that it can be obtained with near-perfect structural quality and has a single isotropic conduction band at 'Γ'. This will simplify the analysis. We also note that pyrite also has a single isotropic conduction band at 'Γ'. (Fig 8)

Table 2: properties as specified by the manufacturer MTI Corporation. Of GaAs samples used for our research

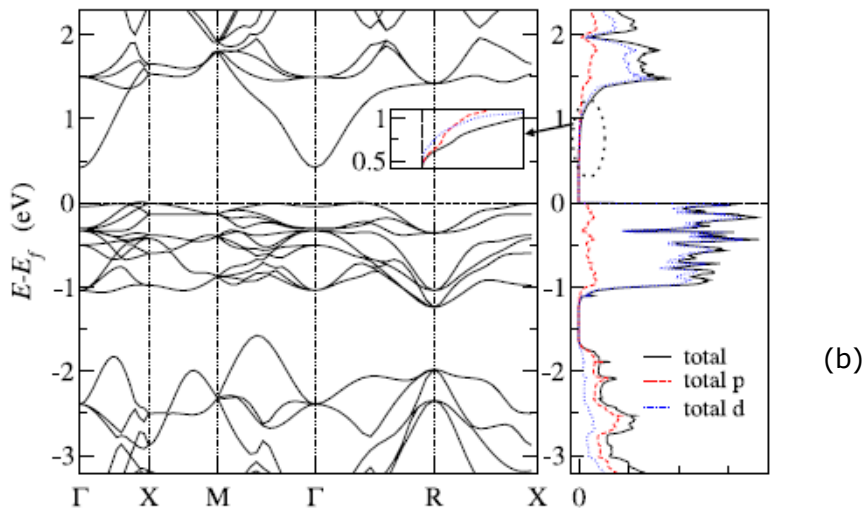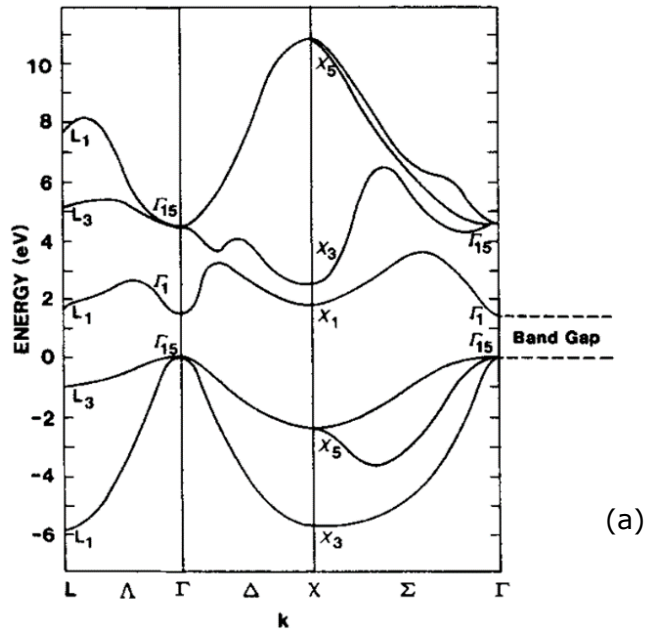| n-type GaAs Sample properties	7.7×10^{16} cm^{-3}	2.7×10^{17} cm^{-3}	1.49×10^{18} cm^{-3}
Type	n	n	n
Dimensions	1 cm X 1 cm X 0.05 cm	1 cm X 1 cm X 0.045 cm	1 cm X 1 cm X 0.035 cm
Doping(cm^{-3})	$(3.8-6.2) \times 10^{16}$	$(3.04-5.98) \times 10^{17}$	$(1.07-1.9) \times 10^{18}$
Resistivity(ohm-cm)	$(2.74-4.24) \, 10^{-2}$	$(3.14-5.34) \, 10^{-3}$	$(1.70-2.37) \, 10^{-3}$
Hall mobility(RT)(Cm^2/V.s)	(3450-3890)	(3330-3850)	(1930-2470)

(a)

(b)

Figure 8: Energy Band diagram of (a) GaAs and (b) pyrite with its density of states[7] , note that the conduction band minima for both of these material is at 'Γ'

For this study, all the samples were obtained from 2"- diameter (100) oriented tellurium doped wafers. The doping concentration were chosen to be well above the metal insulator transition of GaAs (N_D-5.2 x 10^{15}cm^{-3}) so that the carriers don't freeze out at low temperatures. These samples were diced into 1 cm x 1 cm pieces and

degreased with acetone and D.I. water, then etched in a H_2SO_4 (1.5%)+ H_2O_2 (1.5%) solution for 5 min. After that, they were cleaned with acetone and D.I. water.

For the Hall measurements in the Van der Pauw configuration, indium (In) contacts were pressed on GaAs substrates and then annealed at 450°C in a forming gas atmosphere. This method proved to be most consistent way to make ohmic contacts on GaAs[21]. Deposition of Corbino Disk contacts on GaAs is explained in the vacuum deposition section.

NATURAL PYRITE

Bulk pieces of natural pyrite were diced into 1 cm x 1 cm x 1 mm and then polished into mirror-smooth wafers

- a low speed diamond wheel saw (South Bay Tech Inc., Model 650 saw) with a 4" x .012" (10.15 cm x 0.3048 mm) diamond wheel disc (South Bay Tech Inc., Model DWL4121),
- variable speed grinder polisher (Ecomet 3, Buehler),
- 30 μm, 15 μm, 6 μm, 3 μm, 1 μm, 0.25 μm and 0.1 μm lapping paper successively.

Samples were subsequently cleaned with acetone and D.I.-water in an ultrasonic cleaner (Branson Model 2510) for 5 min each, and then blown dry with nitrogen gas.

VACUUM DEPOSITION OF OHMIC CONTACTS

The metal/pyrite contacts and metal/GaAs contacts were formed by thermal evaporation of elemental metals onto natural pyrite and GaAs. These contacts were then used in the Hall, I-V (current-voltage) and magnetoresistance measurements. For these depositions, a substrate holder that can house four 1cm X 1 cm sample was

made using aluminum. For the Van der Pauw configuration and Corbino disk contacts, stainless steel shadow masks were specially made as shown in figure 9. Four holes were drilled on the mask to produce a 1 mm diameter contact in the corner position of a square sample for Hall measurements. The Corbino disk mask produced a 0.254 cm diameter contact in the center and a ring with an inner diameter of 0.635 cm diameter.
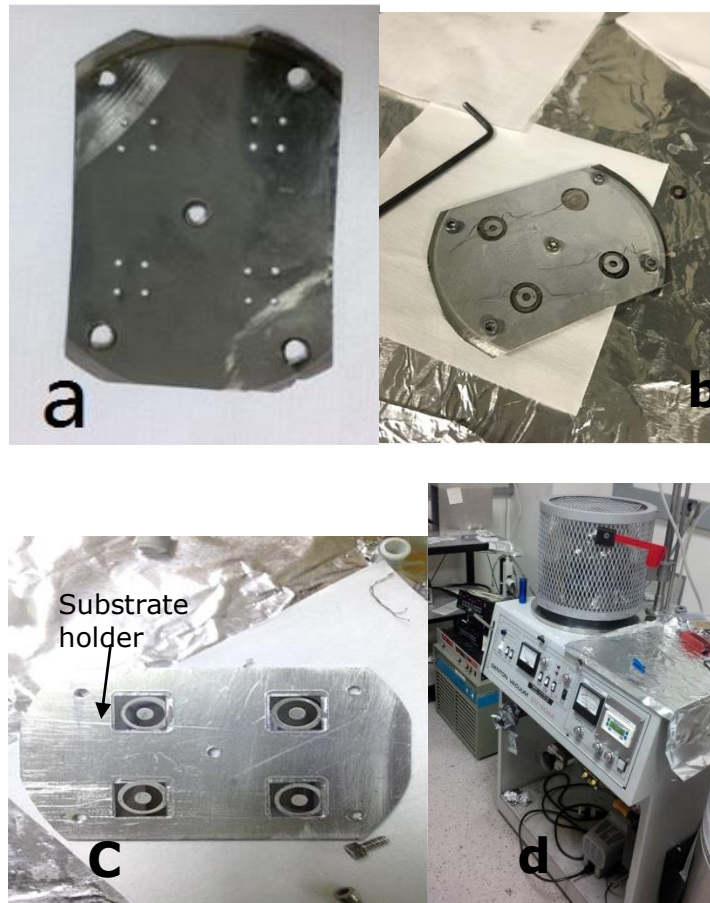

Figure 9: (a) Mask for four point Van der Pauw configuration, (b) mask for depositing Corbino disk configuration, (c) substrate holder with substrates and samples with deposited metal in Corbino disk configuration. (d) Vacuum thermal evaporator system used to deposit metals

In order to form metal ohmic contacts, vacuum thermal deposition was performed using a cryopumped Denton Vacuum (DV-502A) evaporator with a pressure of 10^{-7} Torr. Metals were placed in alumina coated tungsten crucible (R.D. Mathis,

model WBAQ-2 (reaches $1475^{\circ}C$ at 40 Amps)). The time duration for evaporations were estimated using the manufacturer's information for the temperature-current relation for the crucible filament and vapor pressure charts. For cobalt contacts, (RD Mathis, Model WBAQ-2) was used, 40 amps current was sourced, and the length of deposition was 2 min. As for indium contacts, which is very easy to evaporate, the same type of crucible was used, the current was ramped to 30 amps and then held for 1 min. Several hundred angstroms or more were typically deposited. During the evaporation of the Corbino disk contacts, two heating filaments were used to eliminate shadowing from the wires onto the mask.

After the metal contacts were made, samples were glued using Duco-Cement to 44-pin chip carriers (PB-F87049, Evergreen Semiconductor Materials Inc.). Gold wires (99.99% purity) were wire affixed to the metal contacts on the pyrite and to the chip carrier bond pads using conducting silver paste with specified resistivity of 3×10^{-5} ohm-cm(SPI supplies).

RESULTS AND DISCUSSIONS

GALLIUM ARSENIDE

HALL RESULTS

Hall measurements were performed on all three doping levels of GaAs samples at temperature ranging from 4.2 K to 300 K [see figure 10-13] and at fields ranging from 0.3 T to 1 T. The current sourced for all our measurement was 1.5 mA. Hall measurements are performed, in conjunction with the magnetoresistance determinations, in order to determine the scattering factor, μ_H/μ_{MR}. For all the samples measured, the resistivity increased as the temperature decreased

The Hall voltage in all our samples scales linearly with magnetic field which follows the expected Hall theory, thereby validating our measurements.
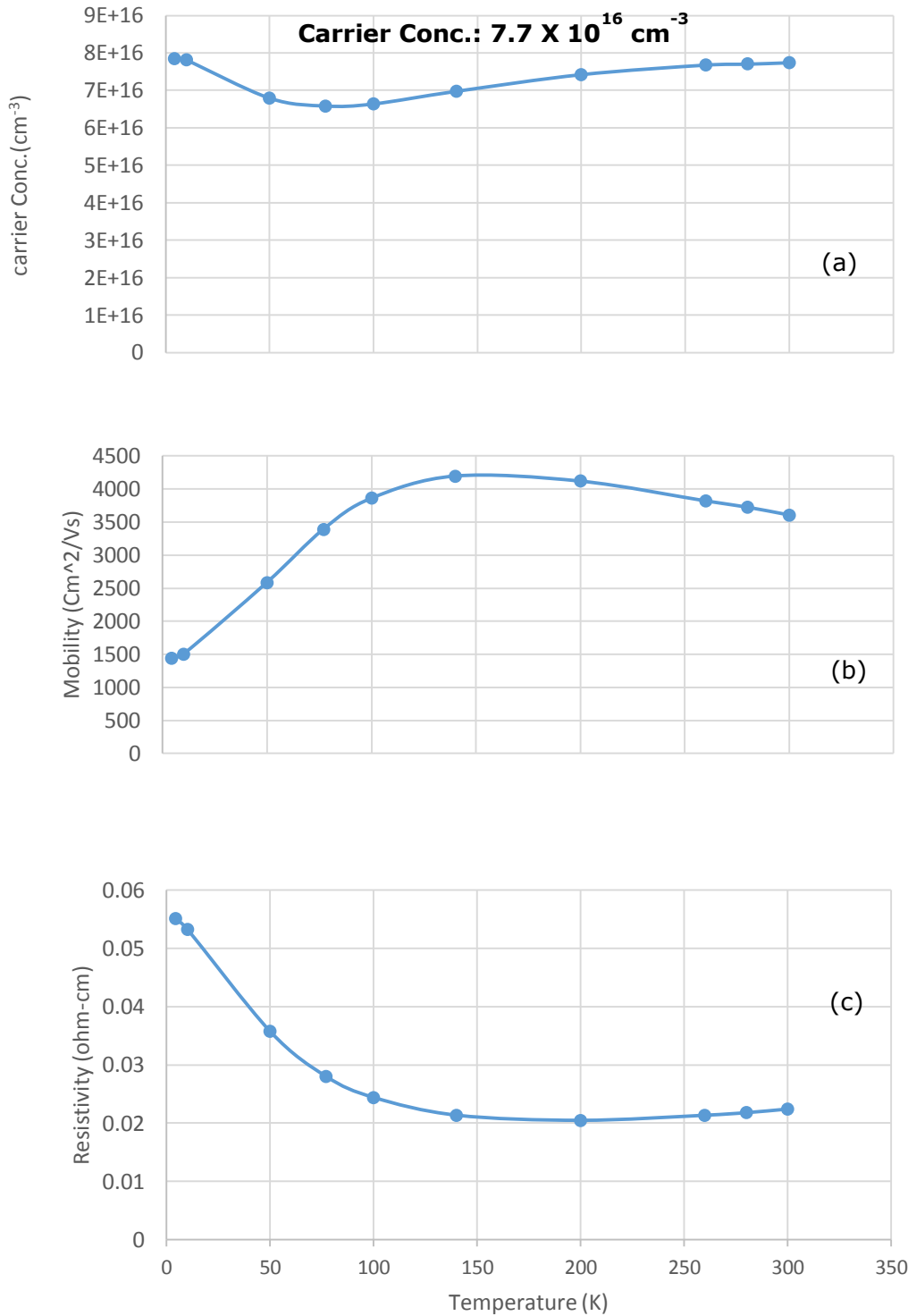
Figure 10: Hall measurement results on the GaAs sample with a room-temperature carrier concentration of ~7.7 X 10^{16} cm^{-3} (a) Temperature versus carrier concentration, (b) Temperature versus Hall mobility (c) Temperature versus resistivity.

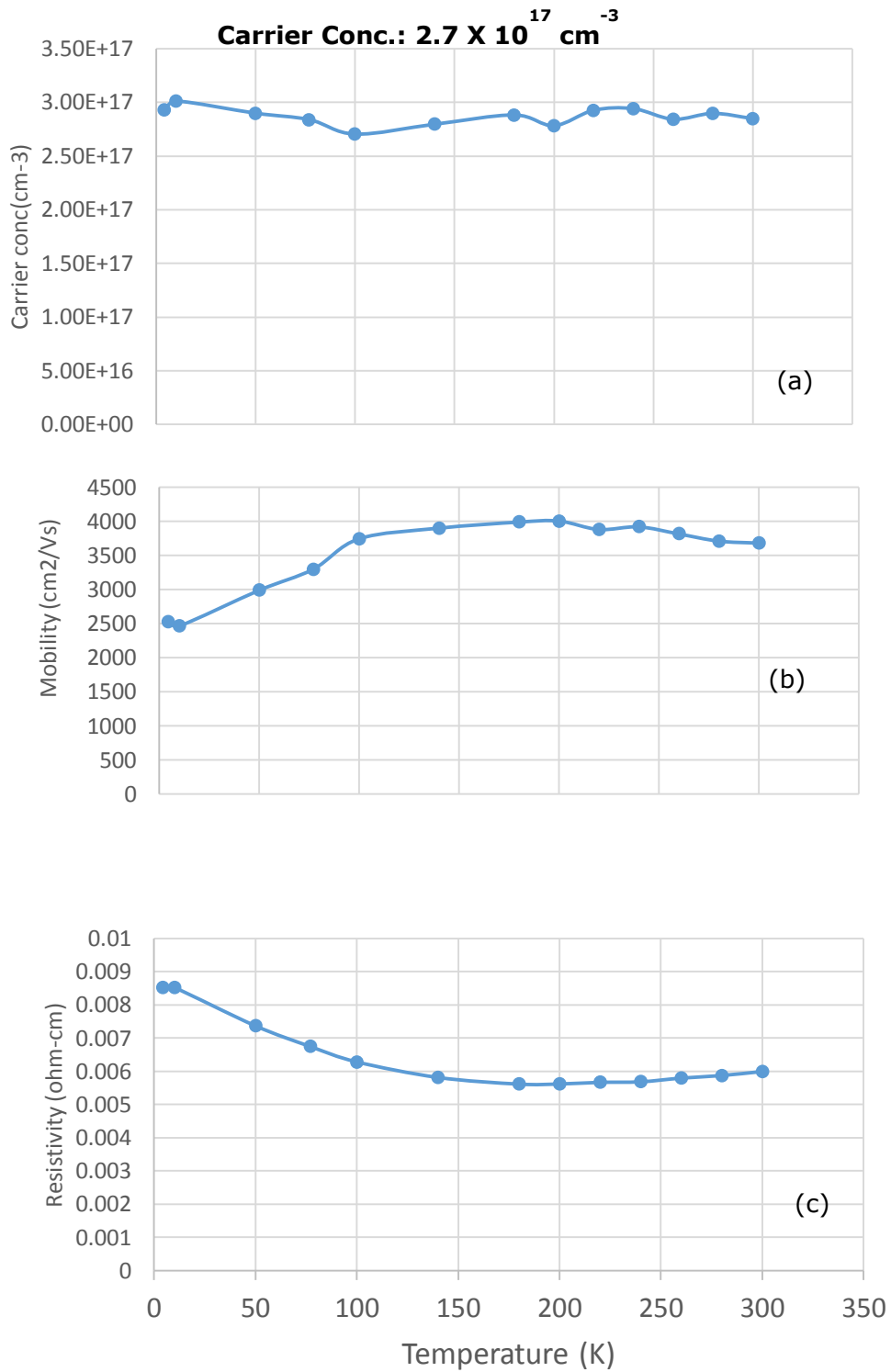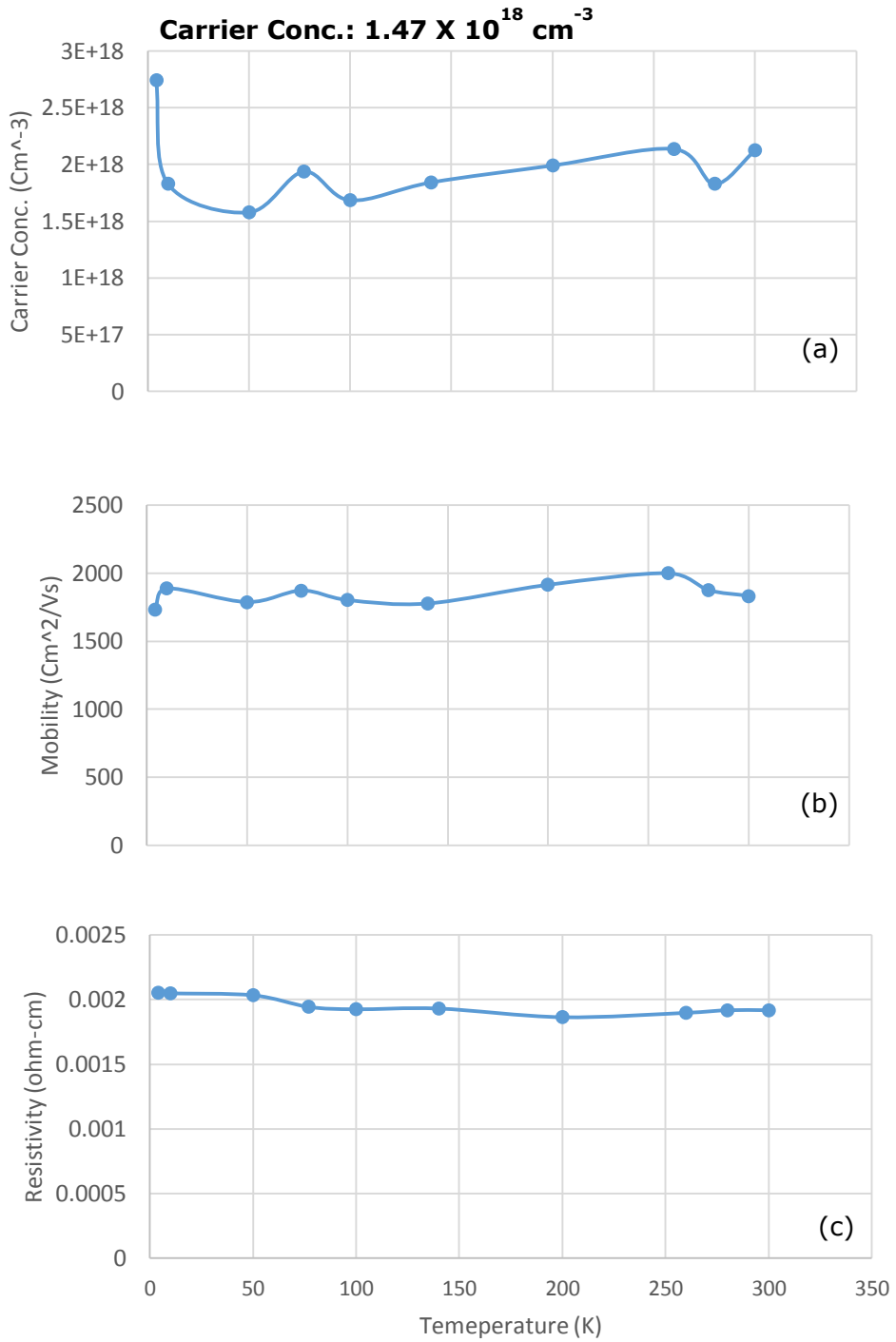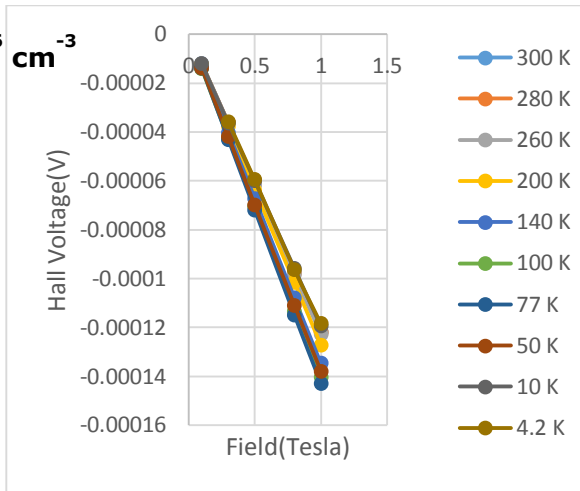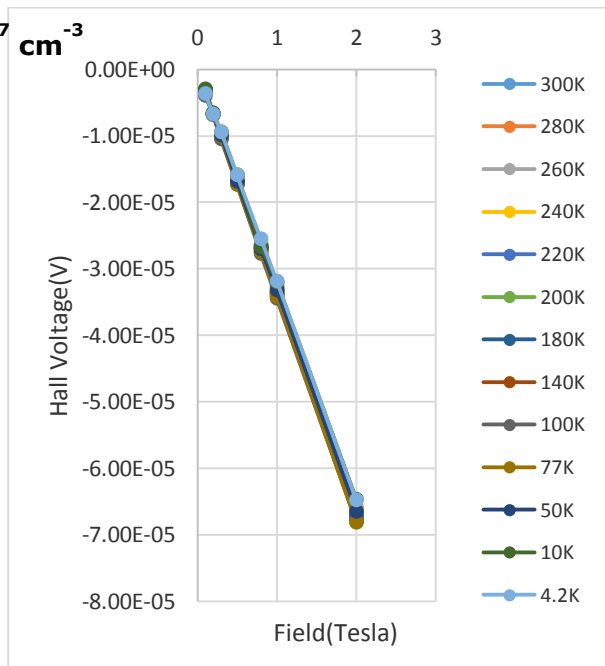Figure 11: Hall measurement results on GaAs sample with a room temperature carrier concentration of ~2.7 X 10^{17} cm^{-3} (a) Temperature versus carrier concentration, (b) Temperature versus Hall mobility (c) Temperature versus resistivity

Figure 12: Hall measurement results on GaAs sample with a room-temperature carrier concentration of ~1.47 X 10^{18} cm^{-3} (a) Temperature versus carrier concentration, (b) Temperature versus Hall mobility (c) Temperature versus resistivity

Carrier conc.: 7.7 X 10^{16} cm^{-3}

(a)

Carrier Conc.: 2.7 X 10^{17} cm^{-3}

(b)

Carrier Conc.: 1.47 X 10^{18} cm^{-3}

(c)
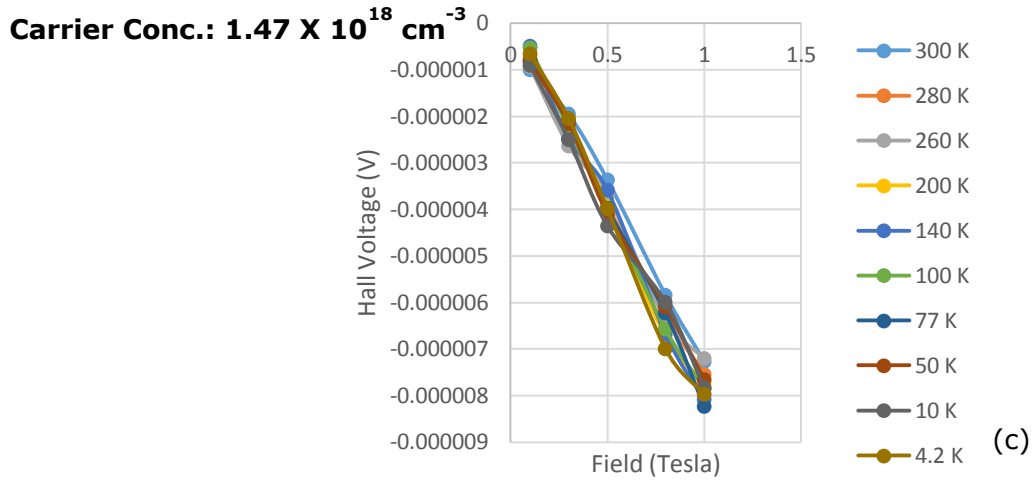
Figure 13: Field versus Hall voltage measurement results in GaAs samples with room-temperature carrier concentrations of (a) 7.7 x 10^{16} cm^{-3}, (b) 2.7 x 10^{17} cm^{-3}, (c) 1.47 x 10^{18} cm^{-3}. Note that the Hall voltages scale linearly with field, validating our measurement results

Our Hall mobilities at 300 K were slightly lower than the reported Hall mobilities

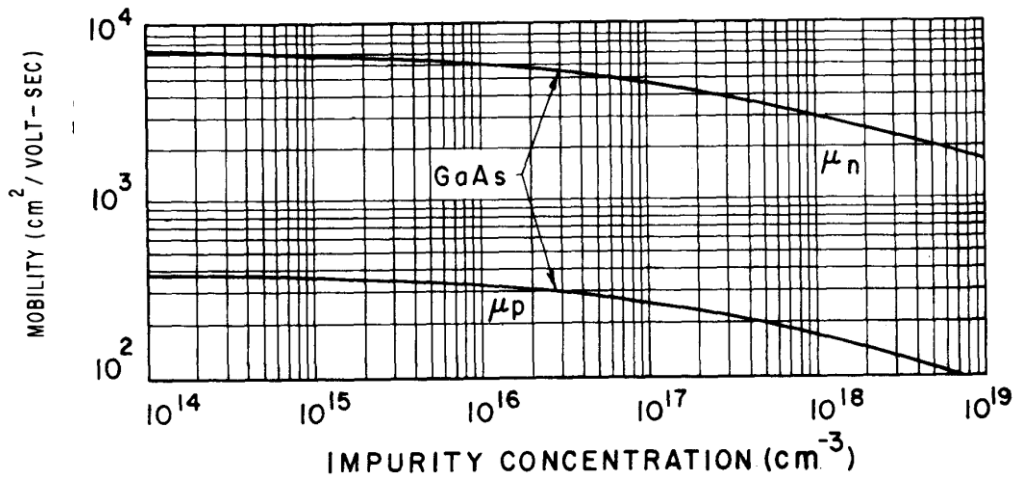by Sze S. M [16]. This suggests that the samples could be slightly compensated

Figure 14: Literature values of experimentally measured mobilities in GaAs as a function of doping concentrations, as summarized by Sze [16]

Table 3: comparing our experimentally measured mobilities with manufacturer specification and those reported by Sze [16]

Measured Carrier Concentration (cm-3)	Measured Hall Mobility @ 300 K (cm2/V.s)	Hall mobility Manufacturer's Specification (cm^2/V.s)	Hall mobility from Sze @ 300 K (cm2/V.s)
7.7×10^{16}	3600	3450-3890	4900
2.7×10^{17}	3680	3330-3850	4000
1.49×10^{18}	1800	1930-2470	2700

MAGNETORESISTANCE RESULTS

In the results described in this section, all the magnetoresistance measurements were performed at a constant DC current of 1.5 mA. The results are summarized in Figure 15-16. The change in $\frac{\Delta R}{R}$ were plotted at various different fields ranging from 0 T to 1 T and these were fitted with a linear fit to determine the coefficient of x.
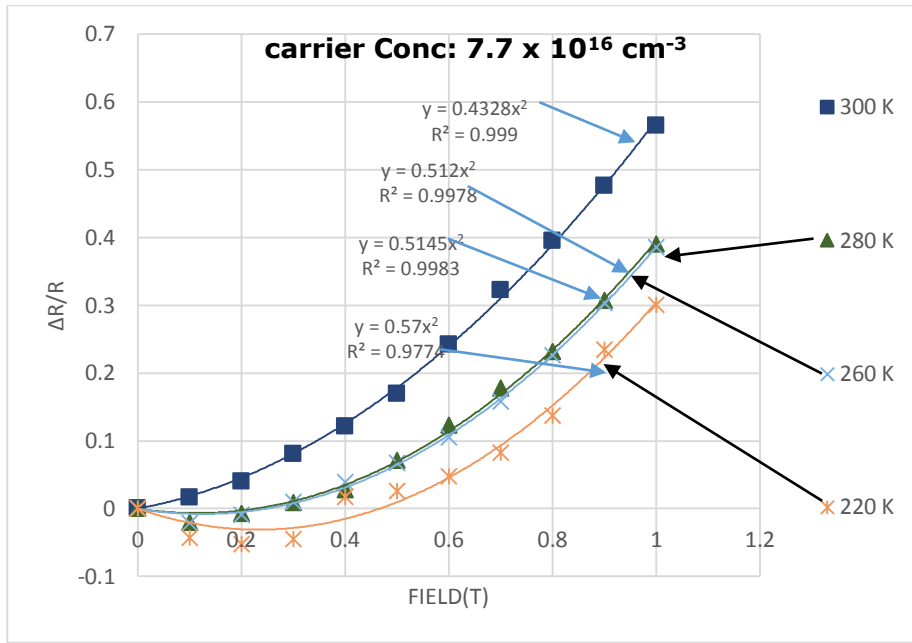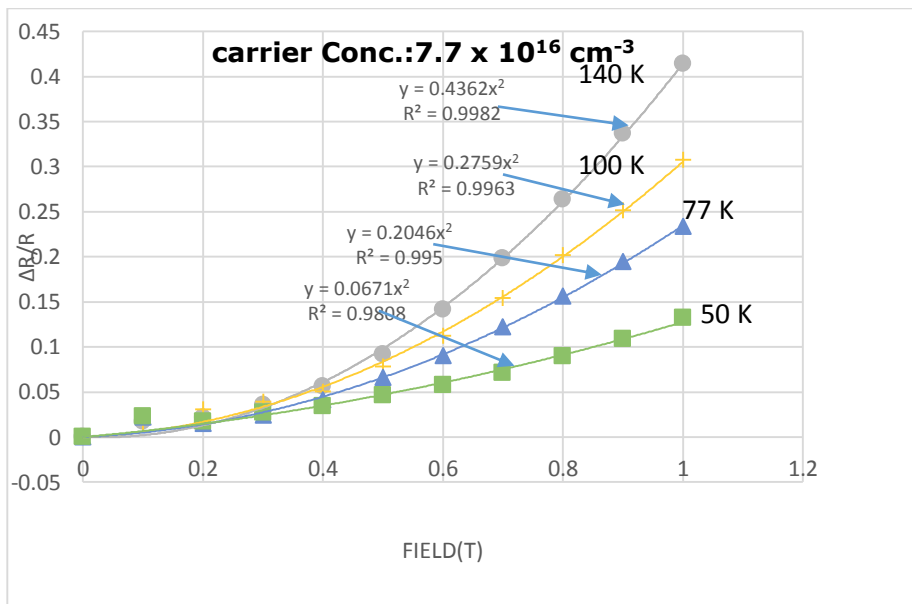
Figure 15: Measurement of results of field versus ΔR/R measurements for the 7.7 x 10^{16} cm^{-3} doped GaAs sample over the temperature ranges (a) 300 K- 220 K and (b) 140 K- 50 K
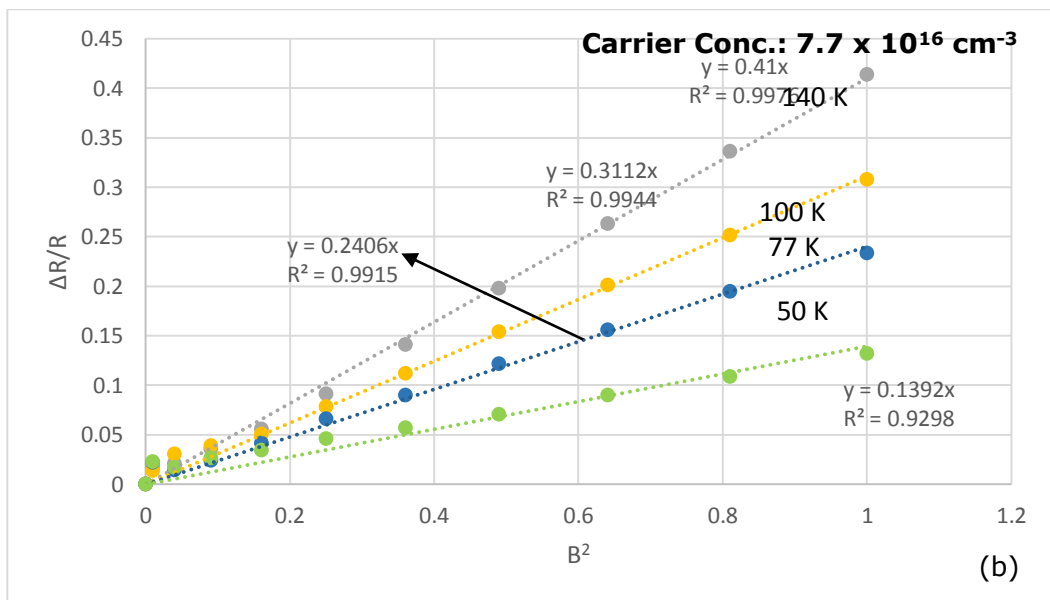
34

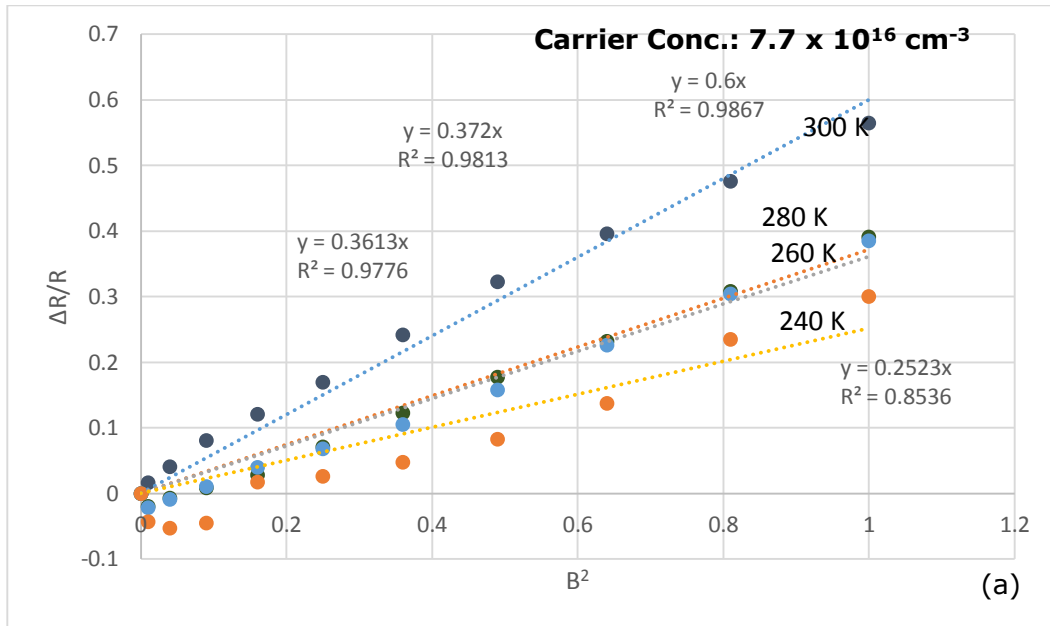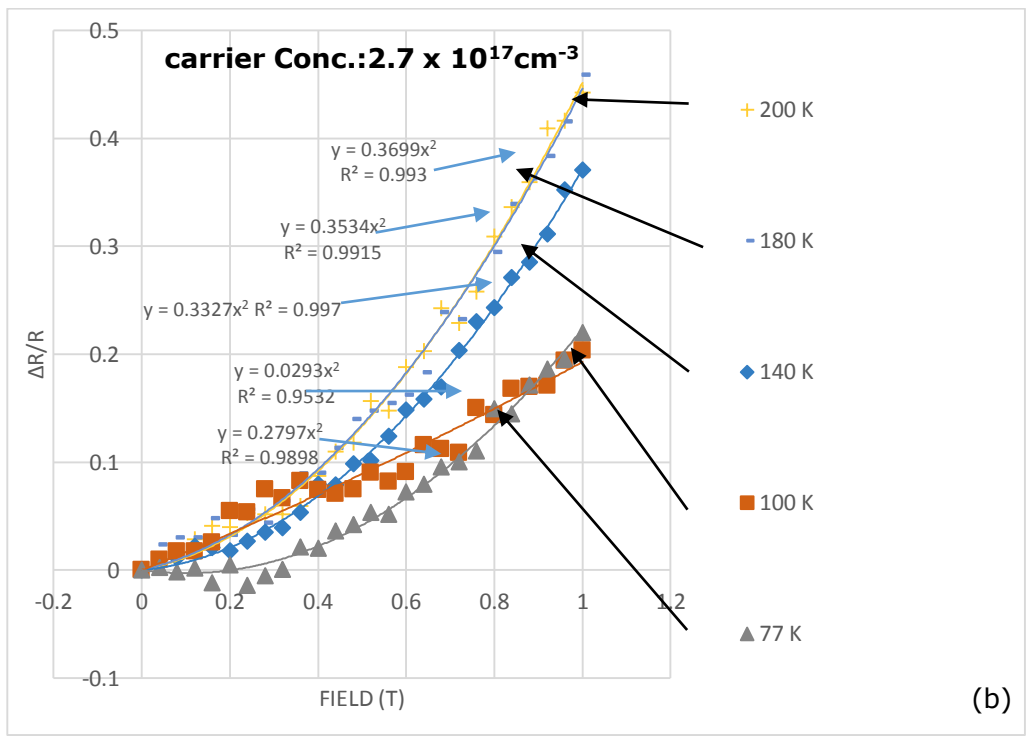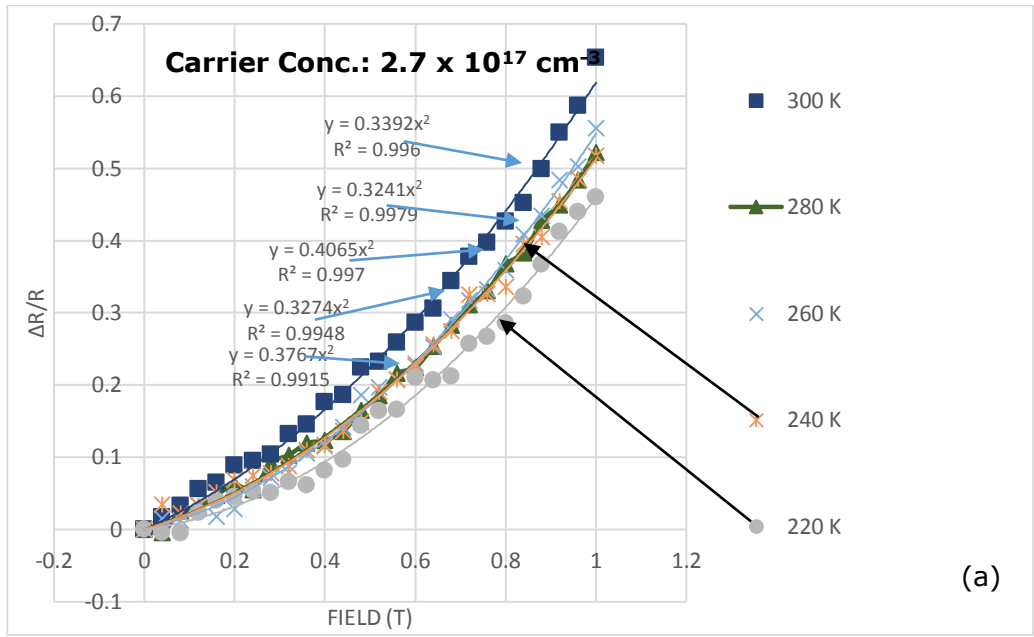Figure 16: Measurement results of ΔR/R versus B^2 for a GaAs sample with a carrier concentration 7.7 X 10^{16} cm^{-3}

Figure 17: Measurement results of the field versus $\Delta R/R$ for the 2.47 x 10^{17} cm^{-3} doped GaAs sample over different temperature ranges (a) 300 K- 220 K and (b) 200 K- 77 K.
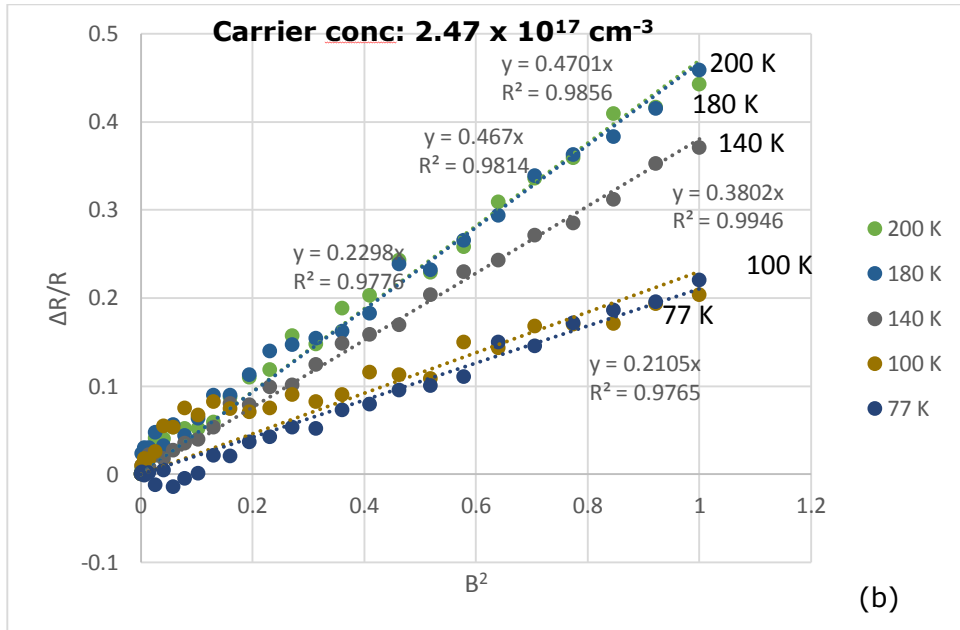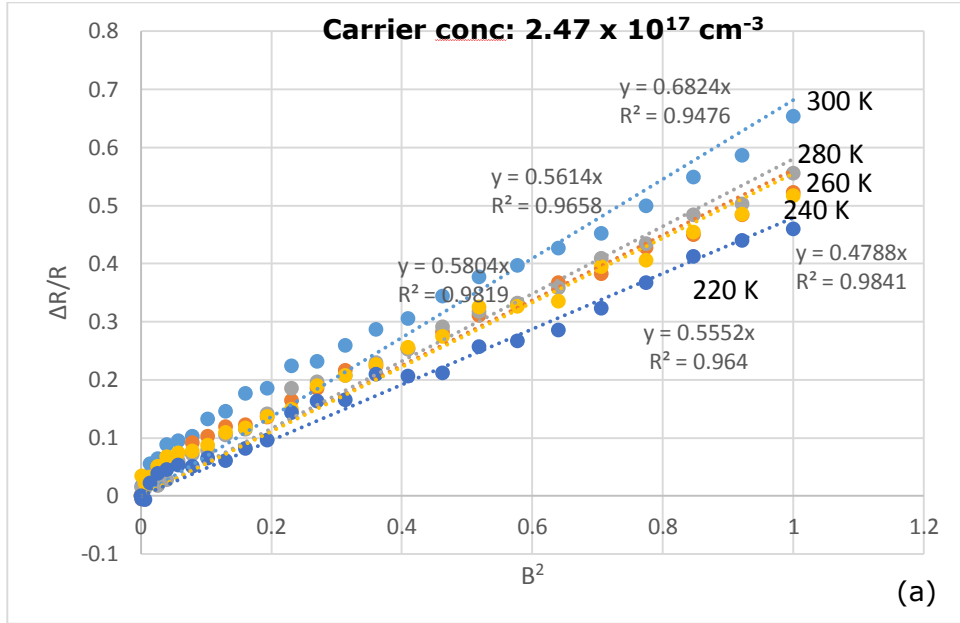
Figure 18: Measurement results of ΔR/R versus B^2 for the GaAs sample with carrier concentration 2.47 X 10^{17} cm^{-3}

At temperatures below 50 K these samples showed negative magnetoresistance. Negative magnetoresistance in heavily doped GaAs has been reported by Arisato Kawabata et.al[22] and Kawaguchi et.al [23-25] and attributed to interference effects during hopping. This is most often observed at low temperatures in highly doped samples
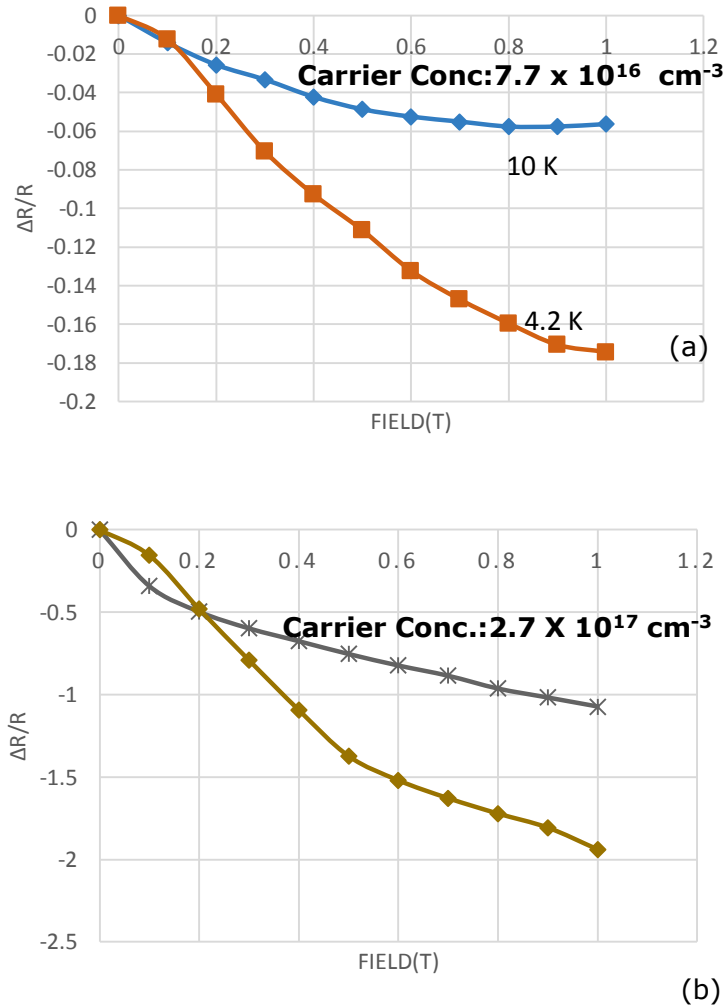

(a)

(b)

Figure 19: Negative magnetoresistance observed at low temperatures in GaAs samples with carrier concentrations of (a) 7.7 X 10^{16} cm^{-3} and (b) 2.47 X 10^{17} cm^{-3}

COMPARISON OF HALL AND MAGNETORESISTANCE MOBILITY

The mobility was calculated using a linear fit of to the $\frac{\Delta R}{R}$ versus magnetic field 'B^2' graphs. From the fit equation, the magnetoresistance mobility (μ_m) can be determined using

$$\mu_m = \sqrt{slope} \qquad\qquad (1.30)$$

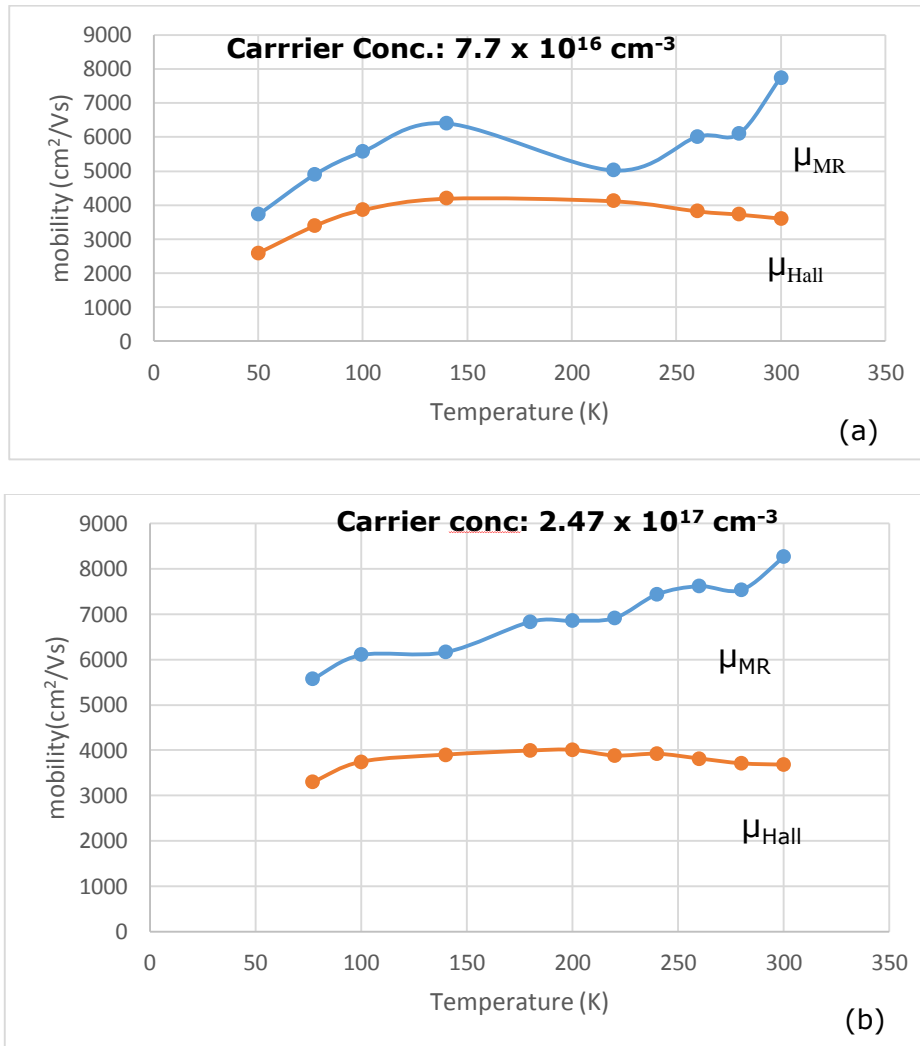The calculated mobility was compared with the measured Hall mobility

(a)

(b)

Figure 20: comparison of measured Hall and Magnetoresistance mobility in GaAs with carrier concentrations of (a) 7.7 X 10^{16} cm^{-3} and (b) 2.47 X 10^{17} cm^{-3}

The scattering factor $'\xi'$ is given by the ratio μ_m/μ_H [26] and the GaAs results are summarized in fig. 21 a and fig. 21 b. The figure shows that ξ is close to 2.1 at 300 K and decreases to 1.21 at 50 K. Jervis T R et al[16] reports that in GaAs with an electron carrier concentration of 6 x 10^{14} cm^{-3} the transport is dominated by ionized impurity scattering and the scattering factor is close to 1.2. This too might have been expected in our highly doped semiconductors.
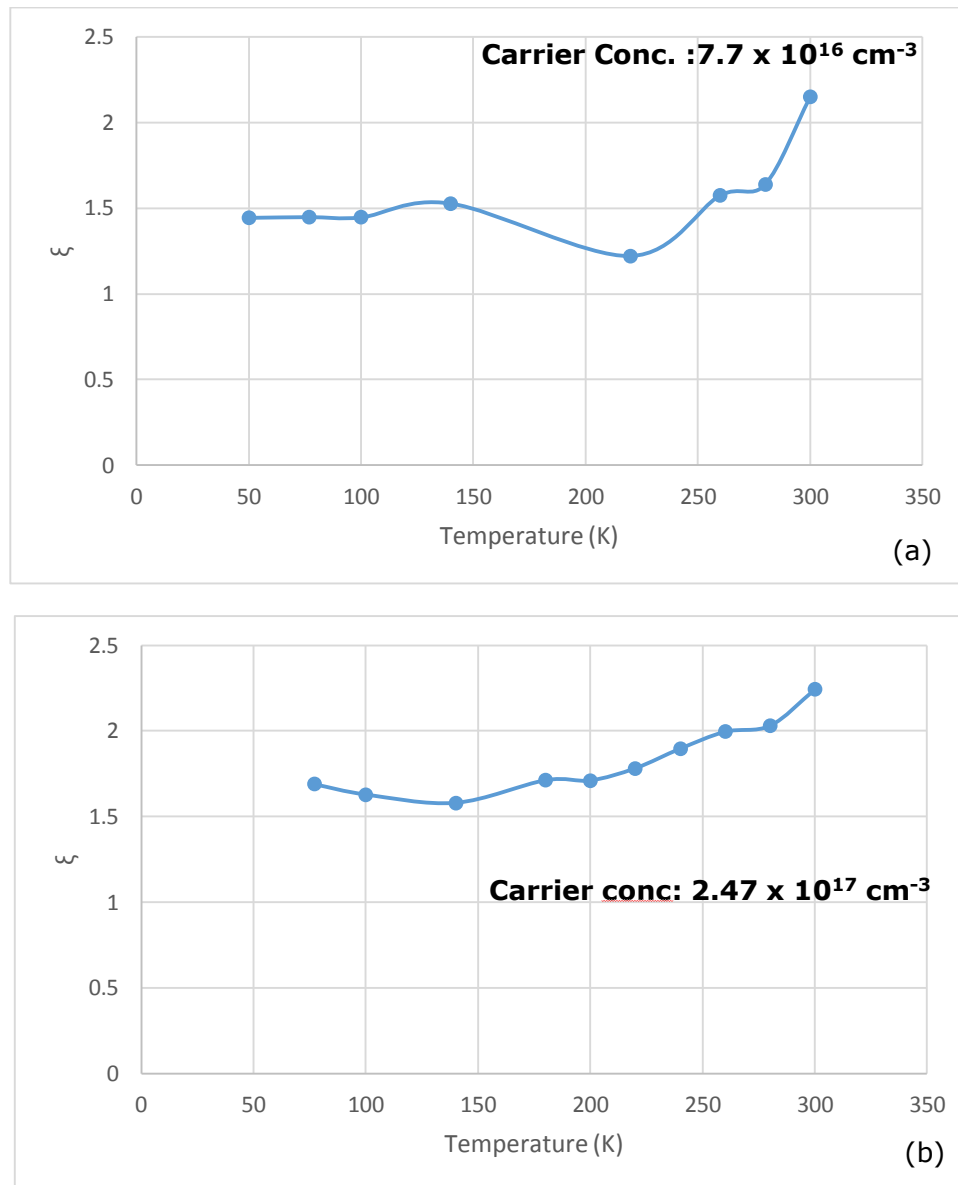

(a)

(b)

Figure 21: Measured scattering coefficient for GaAs samples with carrier concentrations of (a) 7.7 X 10^{16} cm^{-3} and (b) 2.47 X 10^{17} cm^{-3}

NATURAL PYRITE

In this section, we selected the n-type pyrite sample NP#12 with a measured hall mobility of ~25 cm^2/V s with an electron concentration of ~ 10^{19} cm^{-3}

HALL RESULTS

For the sample studied, the resistivities inferred from our van Der Pauw voltages measurements exhibited a decrease in resistivity from room temperature to 100 K and then they remained relatively constant to 4K. Hall measurement showed that the Hall voltages scale linearly with magnetic field except for temperatures below 50 K. At these low temperatures, the contacts were determined to be non-ohmic. The carrier concentration was measured to be ~10^{19} cm-3(see figure 21-22). Altermatt et al has plotted experimental values of mobility for bulk synthetic and natural pyrite. From that graph, we would expect the mobilities of natural pyrite with carrier concentrations of ~10^{19} cm-3 to have mobilities on the order of ~30 cm^2/V.s or less(Fig 20)[27]. Lower than expected mobilities result from the presence of additional scattering, which presumably arises from compensation by native and/or impurity point defects.
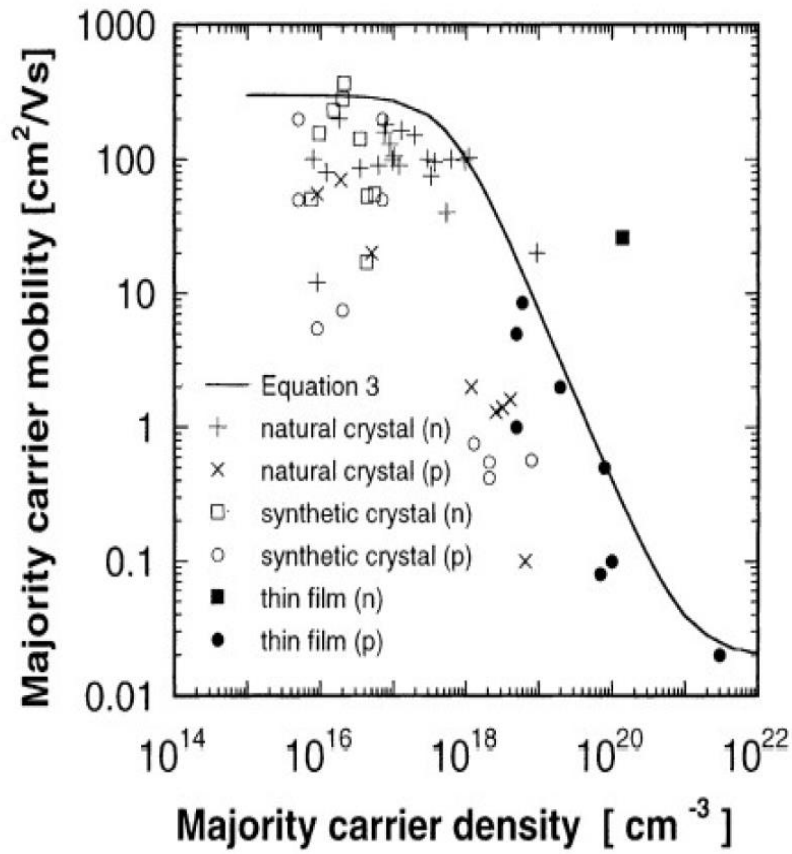
Figure 22: Calculated and experimentally measured mobilities in pyrite thin films as a function of dopant concentration[27]
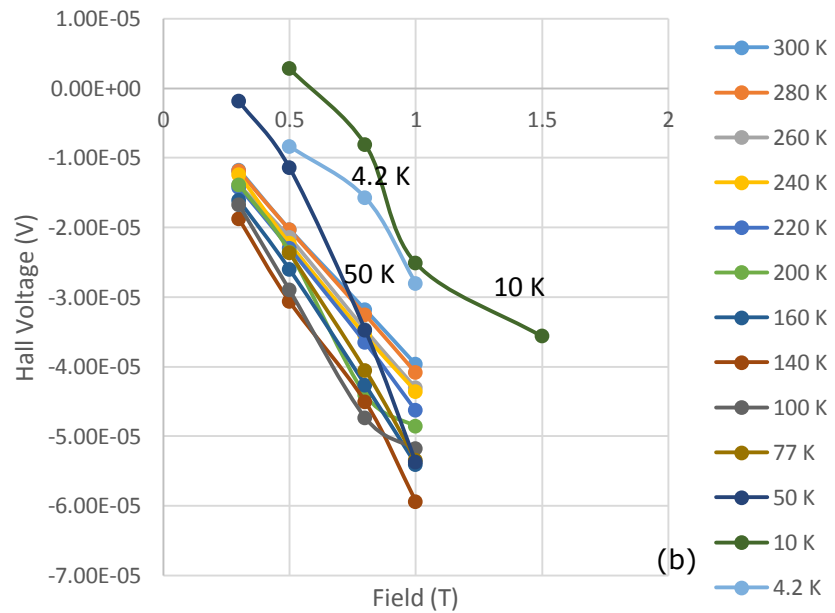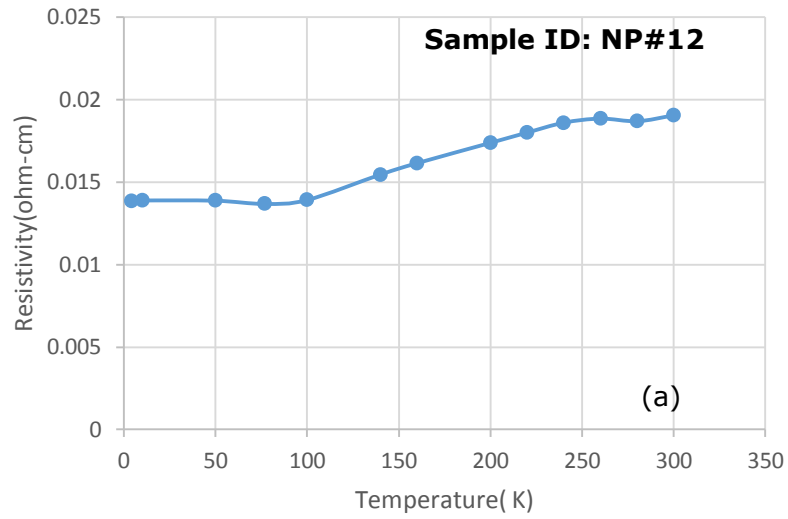
Figure 23: Measurements results of (a) temperature versus resistivity and (b) field versus Hall voltage on pyrite sample NP#12
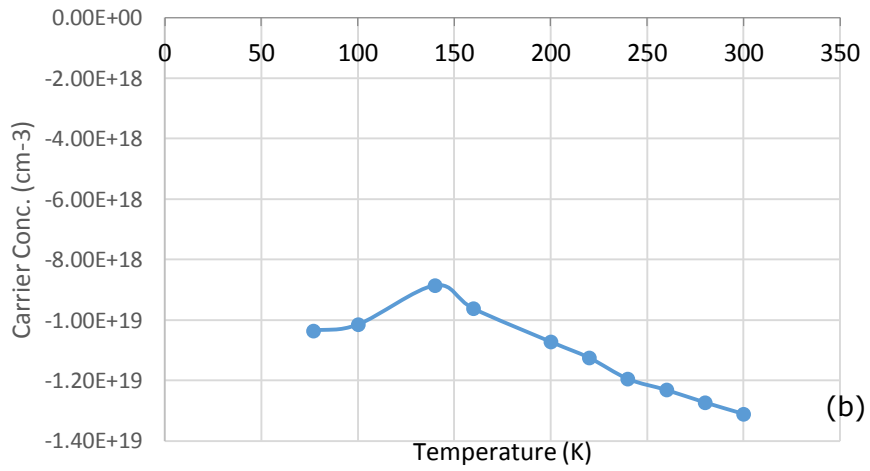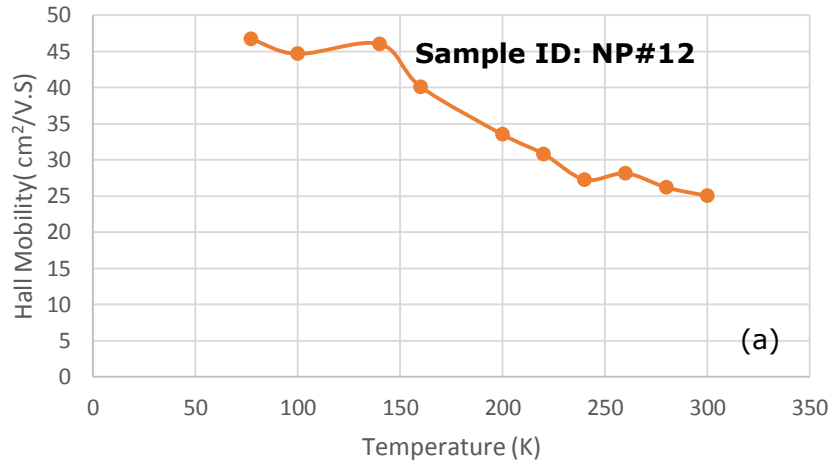
Figure 24: Hall measurement results on pyrite sample NP#12, (a) Temperature versus measured Hall mobility, (b) Temperature versus measured carrier concentration

MAGNETORESISTANCE RESULTS

For this study, I have measured two samples from the NP#12 sample. Cobalt Ohmic contacts in Corbino disk fashion were deposited on the samples in the Corbino disk configuration using thermal deposition. In NP#12_sample 1, IV scans showed Ohmic current-voltage curves at above 100 K and non-rectifying behavior below that, see figure 23. Whereas, in NP#12_sample 2 the IV scans showed the contacts were ohmic and non-rectifying at all temperatures. The MR results on the sample showed a quadratic fit with respect to field, as expected from the theory of magnetoresistance. We will not report results when the contacts are not Ohmic

Cobalt was used for the Ohmic contacts, as it was found to offer the most ideal electrical behavior over other contact metals that we tried. Indium, silver and platinum exhibited Ohmic behavior at room temperature, but not at low temperatures. Aluminum, chromium and iron exhibited Schottky behavior at all measured temperatures.

Since cobalt is ferromagnetic, we made the contacts relatively thin and then only used the high field magnetoresistance results in the analysis to minimize the field generated by the contacts on the mobility determinations
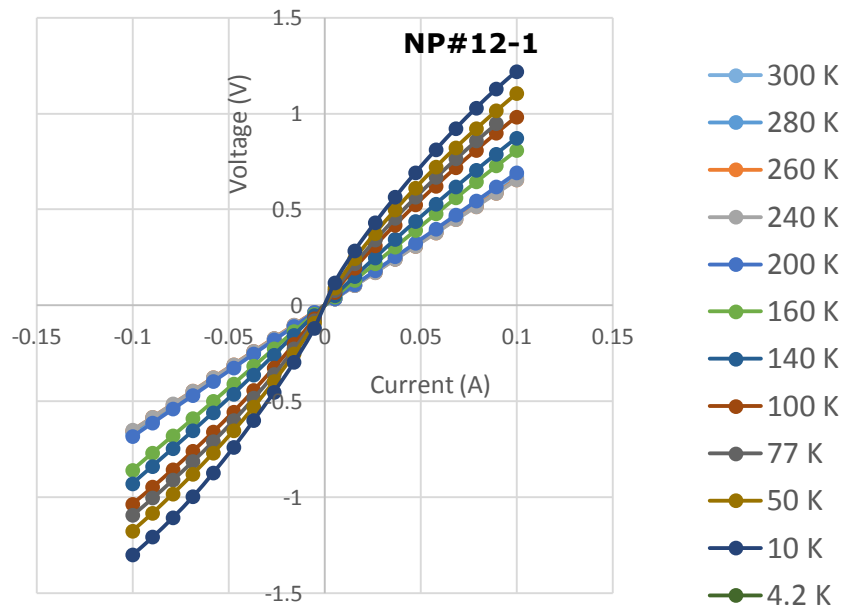
Figure 25: I-V curves of the cobalt contacts deposited on NP#12-1 taken at different temperatures. Note that non-ohmic rectifying behavior observed at temperature below 160 K
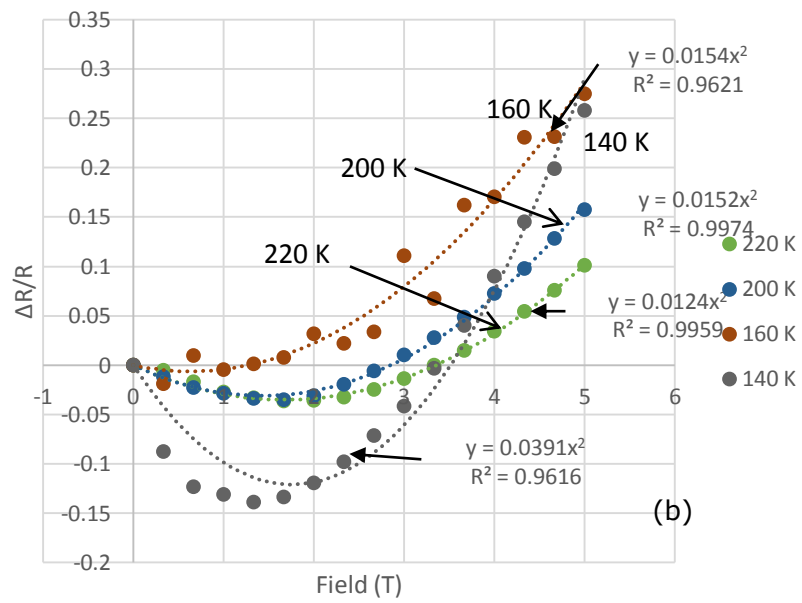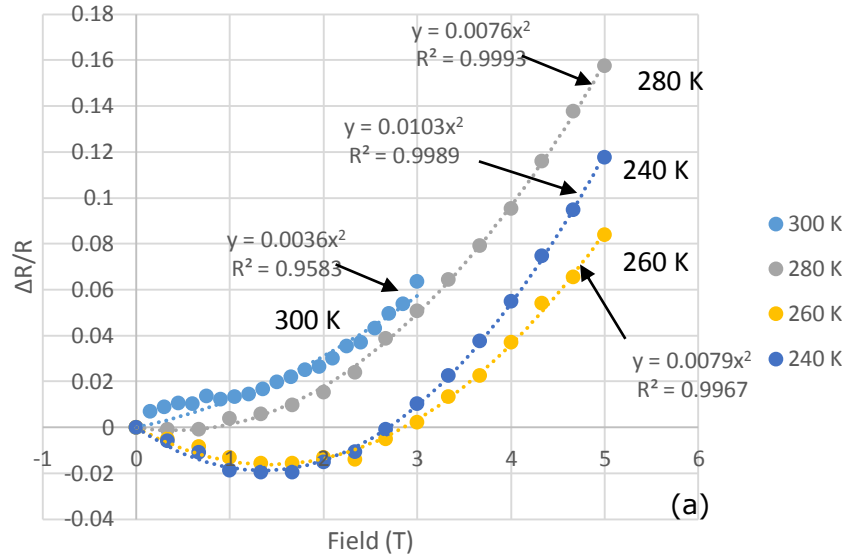
Figure 26: Measurement results of field versus ΔR/R on pyrite sample NP#12-1 over temperature ranges (a) 300 K- 240 K and (b) 200 K- 140 K
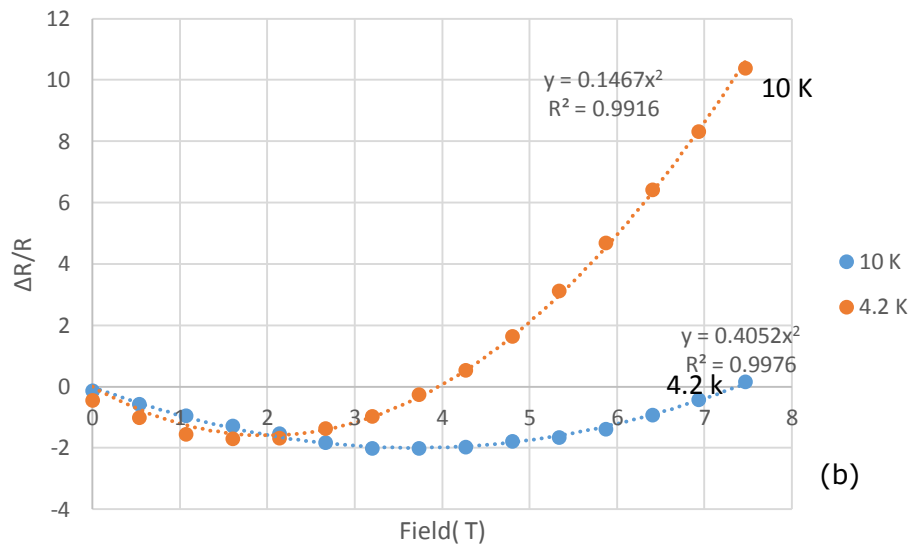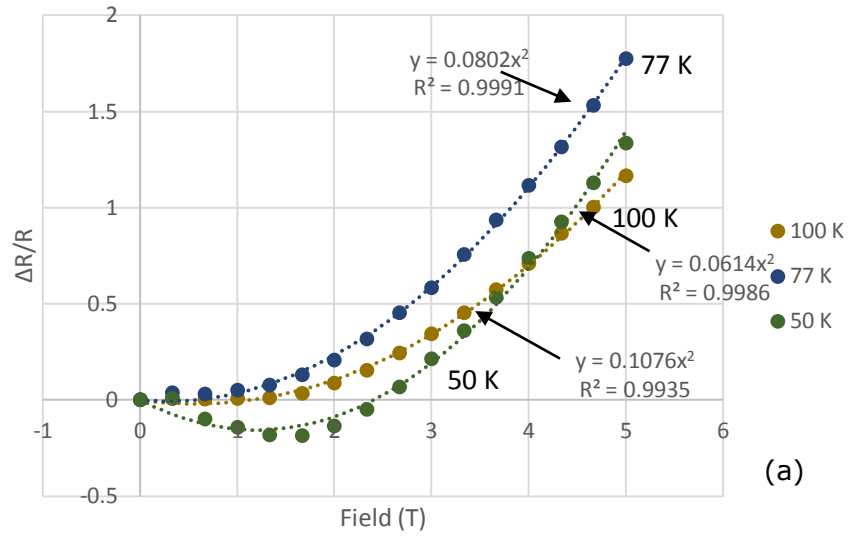
Figure 27: Measurement results of field versus ΔR/R for pyrite NP#12 over the temperature ranges of (a) 100 K- 50 K and (b) 10 K- 4.2 K. Note that the the ΔR/R is > 1 at low temperatures.

Measurement results of ΔR/R versus B^2 curves were plotted for the temperature

range of 300 K-140 K, the region in which the contacts were ohmic
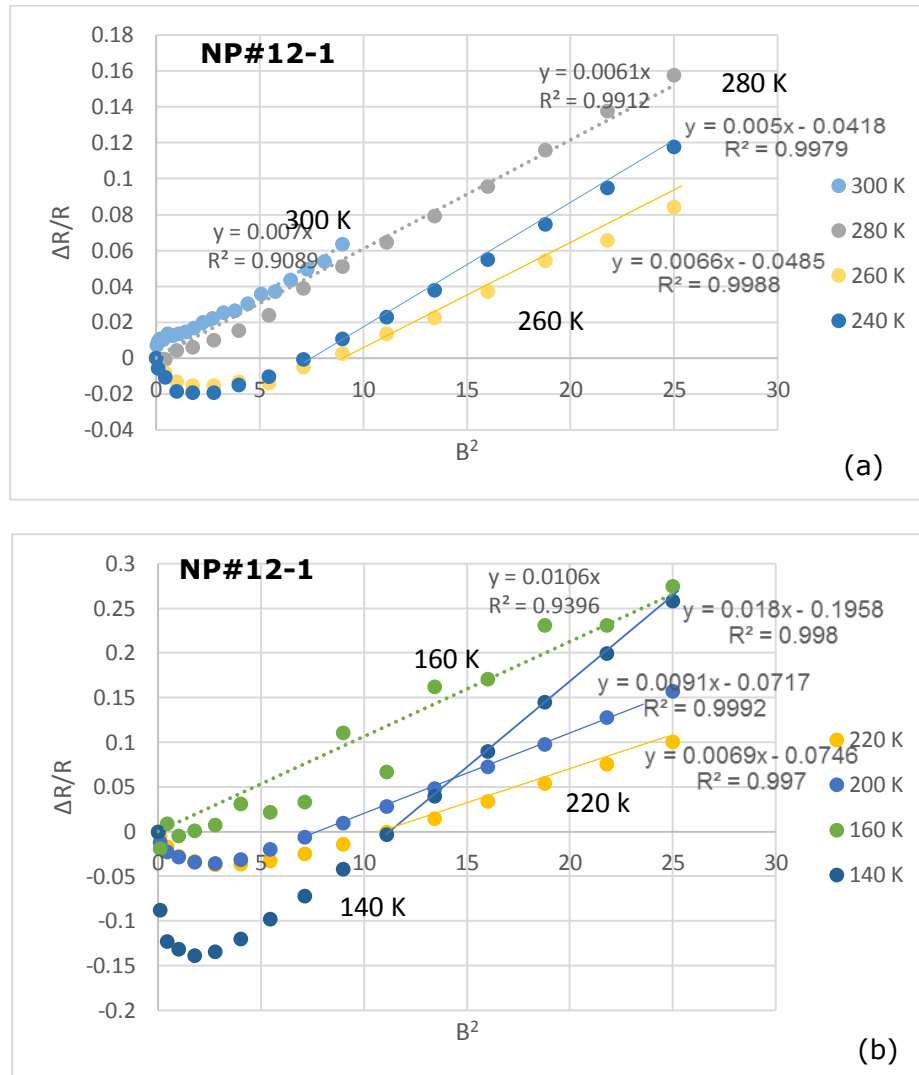
Figure 28: Measurement results of ΔR/R vs B^2 for the pyrite NP#12-1 in the temperature ranges of (a) 300-240 K and (b) 220 K- 140 K. The solid trend lines represent fits at the high field region only and the mobilities are calculated using the coefficient of x.

NP#12 sample 2 (NP#12-2)

(a)

(b)
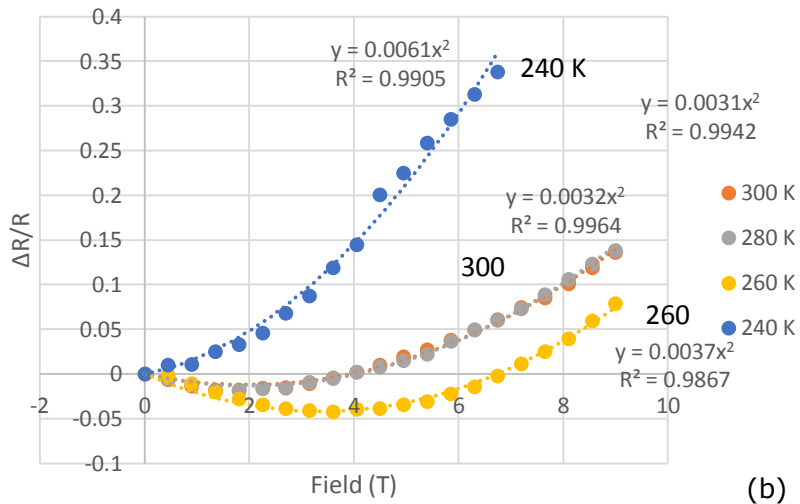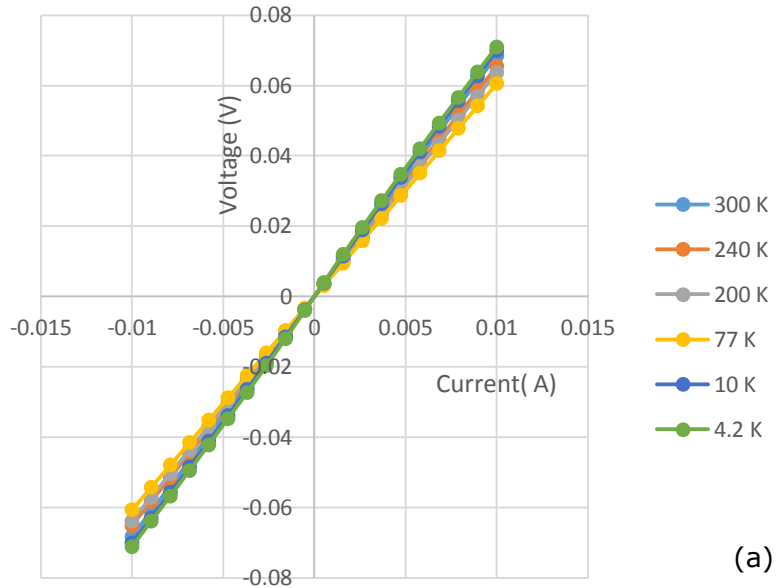
Figure 29: (a) I-V measurement results for the cobalt Corbino contacts deposited on NP#12-2, (b) Field versus ΔR/R results for the NP#12-2 at temperatures of 300 K-240 K. The contacts were found to exhibit ohmic behavior over the entire temperature range, including down to 4.2 K
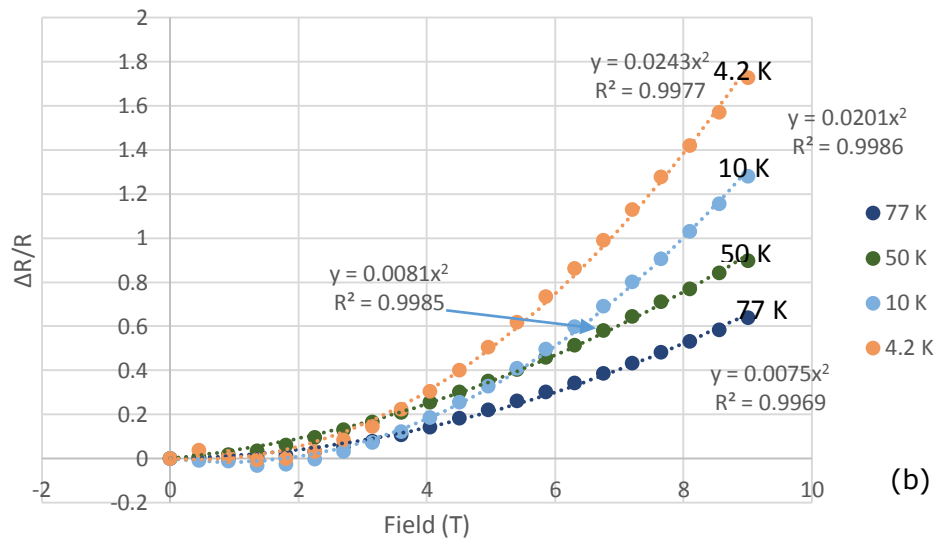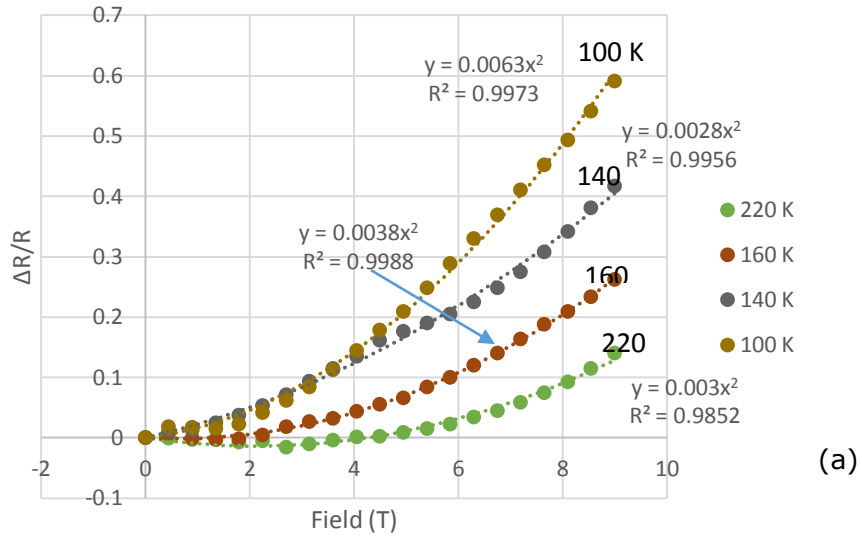
Figure 30: Measurement results for field versus ΔR/R in pyrite sample NP#12-2 over different temperature ranges (a) 220 K- 100 K and (b) 77 K- 4.2 K, observe the ΔR/R is > 1 at low temperatures.
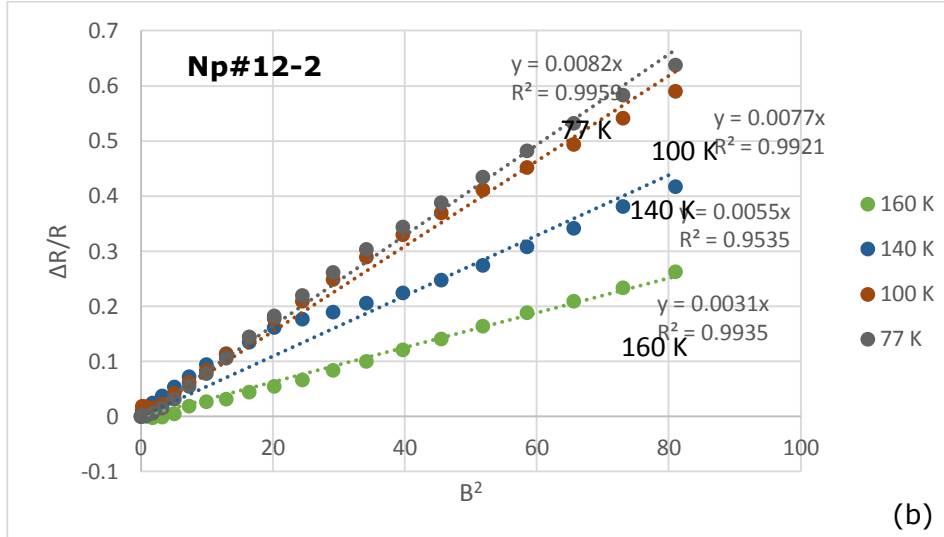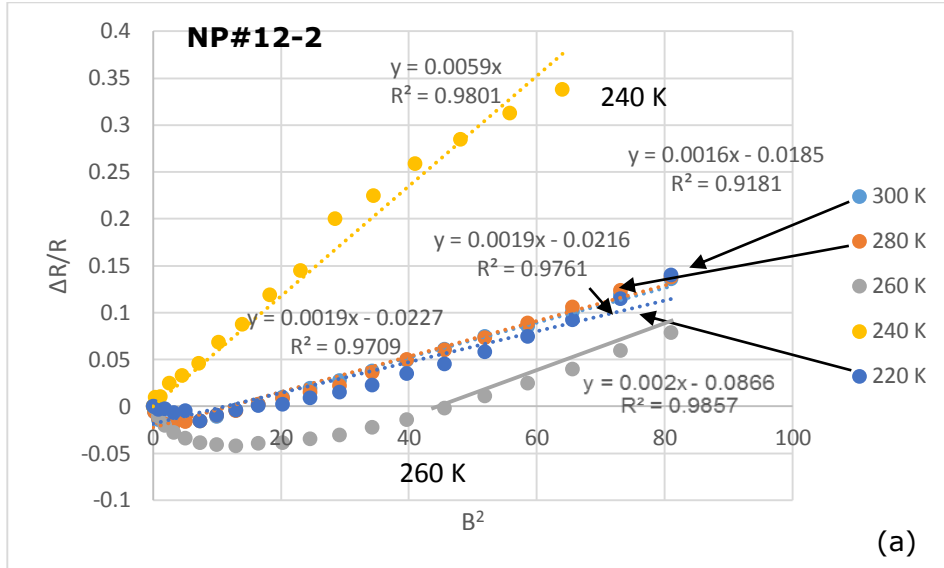
Figure 31: Measurement results of $\Delta R/R$ Vs B^2 for NP#12-2 in the temperature range (a)300 K- 220 K, (b) 160 K – 77 K, solid trend indicate the mobilities at those temperature was calculated at higher fields the mobilities are calculated using the coefficient of x.
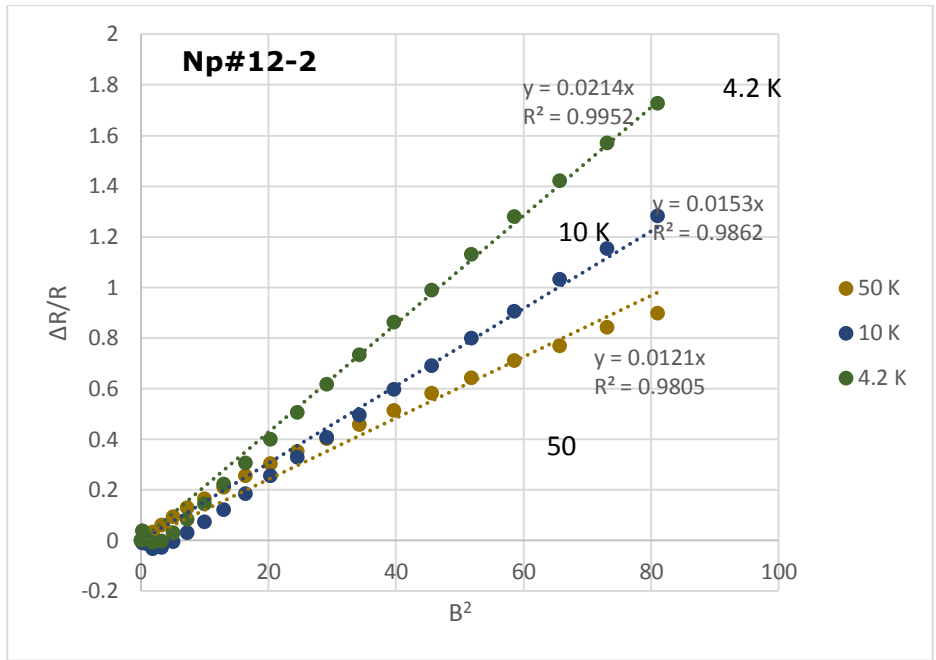
Figure 32: Measurements results of $\Delta R/R$ versus B^2 for pyrite sample NP#12-2 over the temperature range 50 K-4.2 K.

Since we are using the resistance from the 4-point Van der Pauw configuration measurement, we have essentially eliminated the error from contact resistances. In order to determine the effect of heating on our magnetoresistance measurements, I carried out experiments on my NP#12 sample 2 at a number of different current values and magnetic fields as a function of time. The magnetic field was ramped up and then ramped down slowly and no significant systematic errors were found with time, confirming that the effect of heating on the results are negligible. This experiments also confirmed that the measurements values for a given field are repeatable.
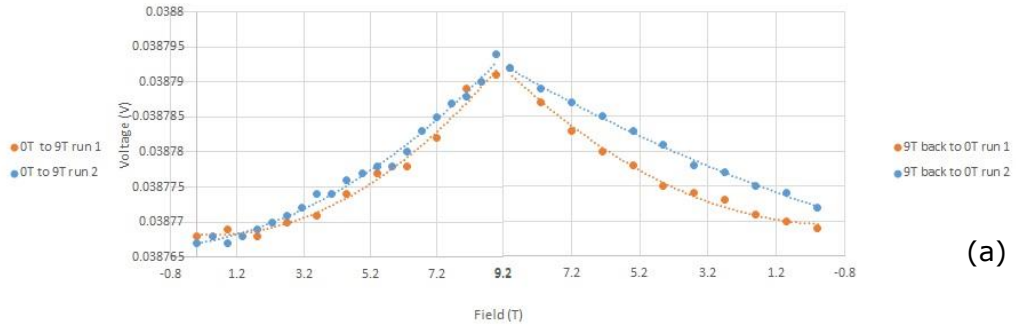
(a)
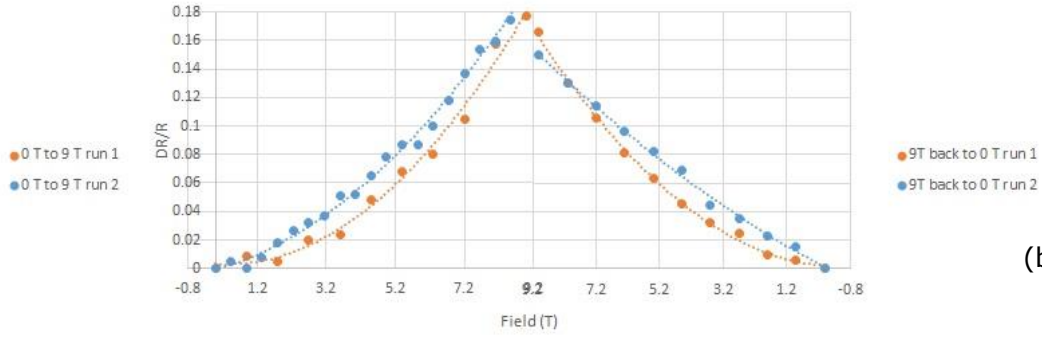
(b)

Figure 33: Measurements on NP#12 sample 2 (a) Field versus voltage, (b) Field versus ΔR/R, indicating that heating effects do not dominate the measurement results.

VSM MEASUREMENTS ON COBALT CONTACTS

Since we used cobalt thin films for our ohmic contacts in our magnetoresistance and Hall measurements, we need to consider whether their ferromagnetic properties significantly affect the measurement results. To evaluate the magnitude of the resulting inhomogeneous magnetic field, we performed VSM measurements (Newport, M406) on pyrite Np#12_1 sample with Co contacts in the Corbino disc configuration.

(a)

(b)
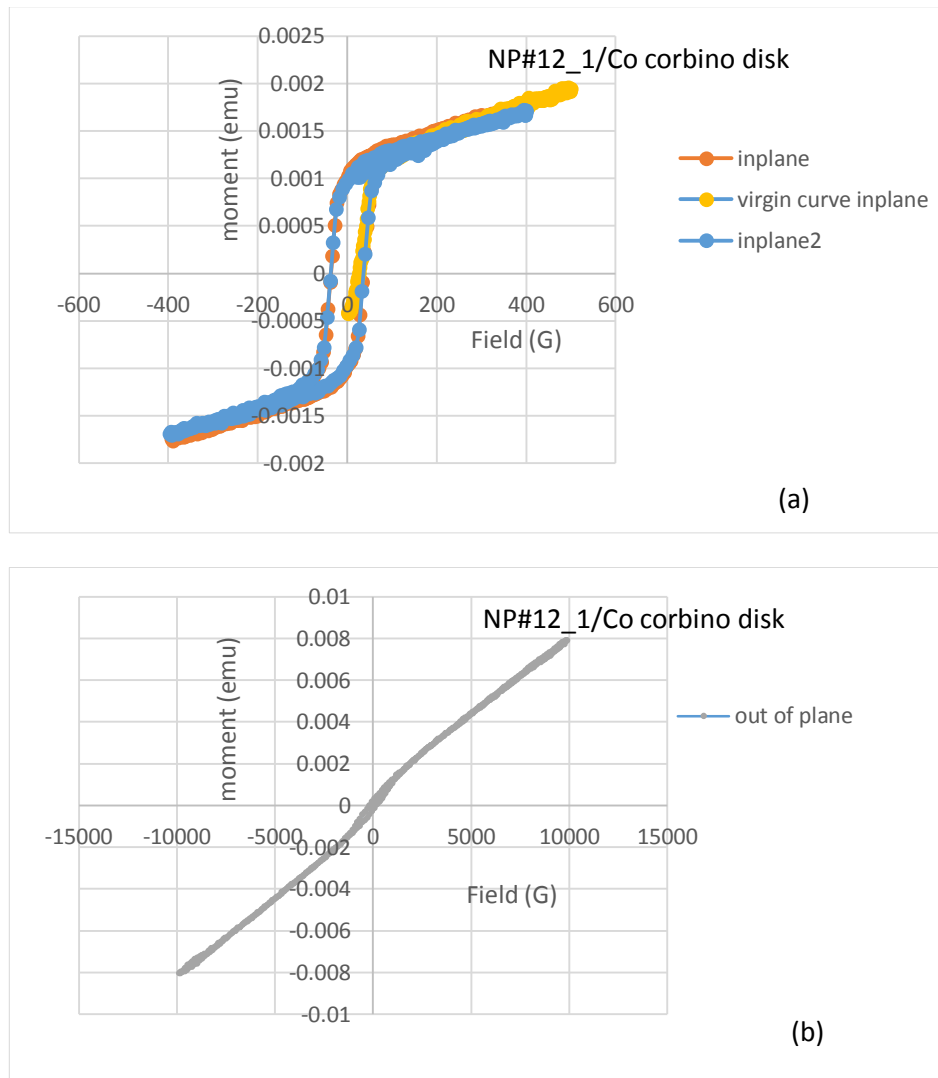
Figure 34: VSM Measurements on NP#12_1 (a) an in plane Moment versus Field (G) (b) an out of plane Moment versus field

The VSM measurements indicate that the in plane coercive field is ~100 Oe, indicating that there will be some stray fields present between the contacts even without an applied field. It also indicates that the hard magnetic axis is out of plane and large. At small fields of say less than 2,500 Gauss, we would expect the contact's contribution to the field to decay with a 1/r dependence from the edge of the contact and contribute a significant field only within a distance of a few times the film thickness. This distance is roughly 2 orders of magnitude smaller than that between contacts. Thus, we would not expect this to cause a significant error in our measurements. However, at high fields, the dipolar field of the contacts could influence the measurements over that entire region between contacts and could have introduced an error of as much as a factor of ~50% in the mobility determinations.

COMPARISION OF HALL AND MAGNETORESISTANCE MOBILITY

The measured mobilities for samples Np#12 sample 1 and Np#12 sample 2 using the magnetoresistance technique were measured to be ~600 cm^2/V·S at 300 K. As the temperature decreased, the mobilities increased to slightly above 1000 cm^2/V·s at low temperatures.
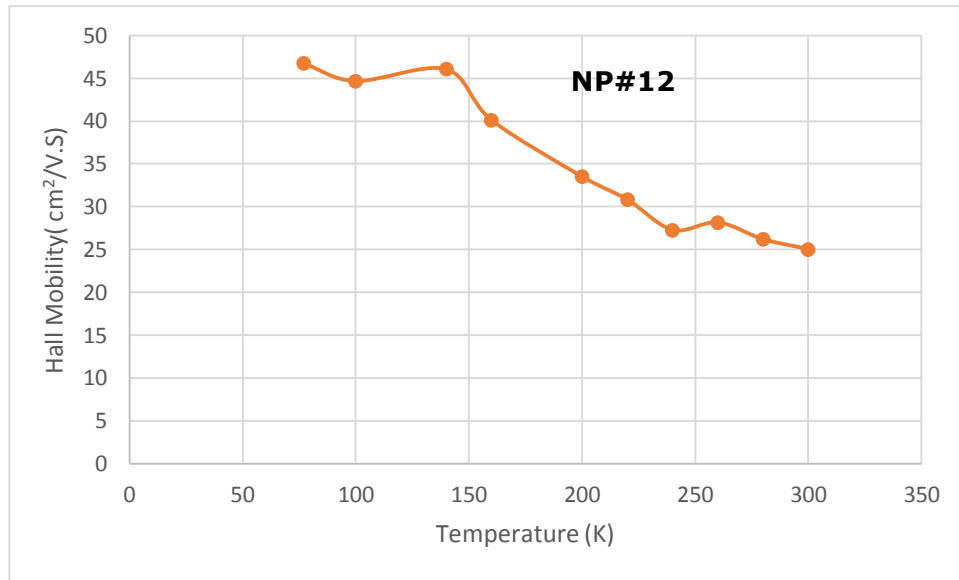
Figure 35: Temperature versus measured Hall mobility for pyrite sample NP#12
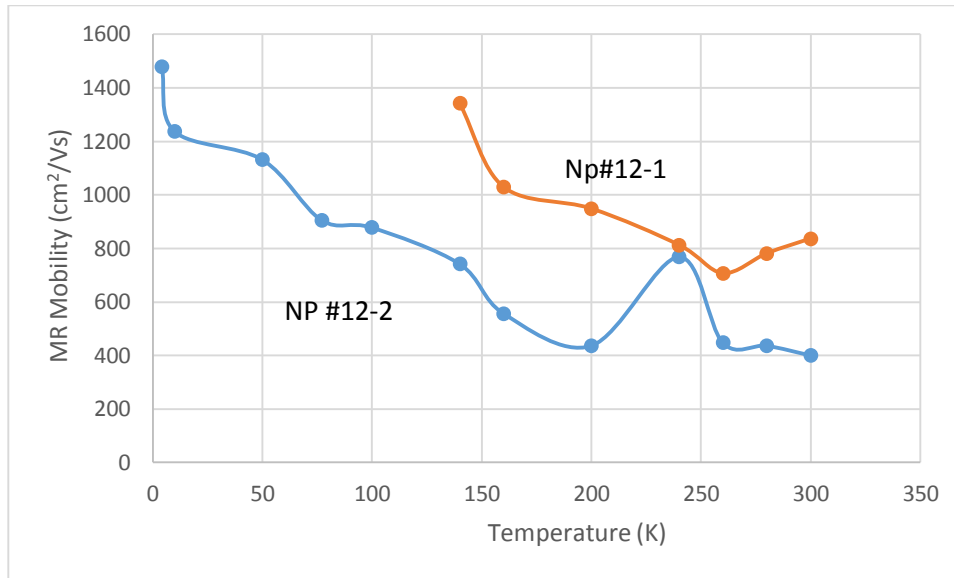
Figure 36: Temperature versus calculated magnetoresistance mobility in NP#12-1 and Np#12-2
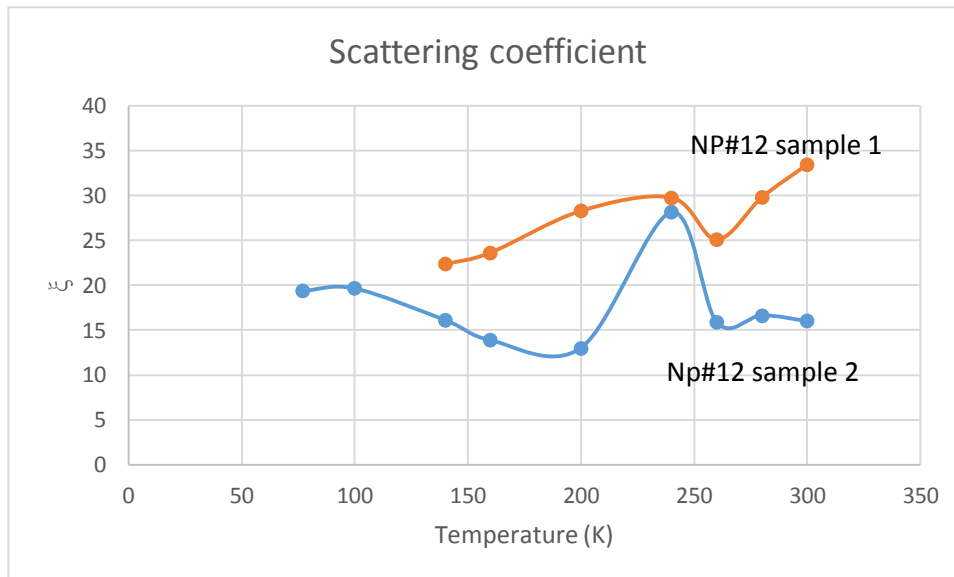
Figure 37: The experimentally determined Scattering coefficient in for the Natural pyrite samples NP#12-1 and NP#12-2.

CONCLUSIONS

I have carried out a systematic study to determine mobilities of GaAs and natural pyrite using the method of geometrical magnetoresistance and compare them to Hall effect determination. The effect of contact resistance on the magnetoresistance measurements were minimized by using the zero-field resistance values from Van der Pauw measurements. The scattering factor, as defined to be the ratio of the magnetoresistance and Hall mobilities, of GaAs was determined to be ~ 2.1 at 300 K and ~1.2 at lower temperatures. This indicates that the sample transport is dominated by impurity scattering. Negative magnetoresistance was observed at lower temperatures in lightly-doped GaAs, at higher temperatures in highly-doped GaAs. In the case of natural pyrite, the scattering factor was found to be around 20 at 300 K and decreased as the temperature decreased. The negative magnetoresistance is enhanced at lower temperatures with $\frac{\Delta R}{R}$ found to exceed unity at lower temperatures.

FUTURE WORK

As we were able to measure mobilities using the Corbino configuration in samples with Hall mobilities as low as 24 cm^2/V.s, we can use this technique to measure the carrier mobilities in pyrite thin films and other highly resistive materials.

This technique can be used to obtain an improved understanding of transport properties of pyrite produced by our group's recently developed sequential evaporation technique and by other methods.

We also hope this work inspires additional work in the negative magnetoresistance, as a detailed understanding of the mechanisms involved has not been firmly established.

Co contacts were used in the pyrite magnetoresistance measurements because they exhibited the lowest resistance Ohmic contacts down to cryogenic temperatures. As the magnetic nature of our Co contacts can influence the field at small applied magnetic fields, we plan to confirm our results using non-magnetic metal contacts such as indium (In) or Silver (Ag).

REFERENCES

1.   Ennaoui, A., et al., *Iron disulfide for solar energy conversion.* Solar Energy Materials and Solar Cells, 1993. **29**(4): p. 289-370.

2.   Murphy, R. and D.R. Strongin, *Surface reactivity of pyrite and related sulfides.* Surface Science Reports, 2009. **64**(1): p. 1-45.

3.   Yu, L.P., et al., *Iron Chalcogenide Photovoltaic Absorbers.* Advanced Energy Materials, 2011. **1**(5): p. 748-753.

4.   Oertel, J., et al., *Growth of n-type polycrystalline pyrite (FeS2) films by metalorganic chemical vapour deposition and their electrical characterization.* Journal of Crystal Growth, 1999. **198–199, Part 2**: p. 1205-1210.

5.   Lichtenberger, D., et al., *Optical, electrical and structural properties of polycrystalline iron-pyrite (FeS2) layers deposited by reactive DC magnetron sputtering.* Applied Surface Science, 1993. **70**: p. 583-587.

6.   Puthussery, J., et al., *Colloidal Iron Pyrite (FeS2) Nanocrystal Inks for Thin-Film Photovoltaics.* Journal of the American Chemical Society, 2011. **133**(4): p. 716-719.

7.   Vahidi, M., et al., *Growth of epitaxial pyrite (FeS2) thin films using sequential evaporation.* Acta Materialia, 2013. **61**(19): p. 7392-7398.

8.   Birkholz, M., et al., *Sulfur deficiency in iron pyrite and its consequences for band-structure models.* Physical Review B, 1991. **43**(14): p. 11926-11936.

9.   Hu, J., et al., *First-principles studies of the electronic properties of native and substitutional anionic defects in bulk iron pyrite.* Physical Review B, 2012. **85**(8): p. 085203.

10.   Sharp, K. and F. Matschinsky, *Translation of Ludwig Boltzmann's Paper "On the Relationship between the Second Fundamental Theorem of the Mechanical Theory of Heat and Probability Calculations Regarding the Conditions for Thermal Equilibrium" Sitzungberichte der Kaiserlichen Akademie der Wissenschaften. Mathematisch-Naturwissen Classe. Abt. II, LXXVI 1877, pp 373-435 (Wien. Ber. 1877, 76: 373-435). Reprinted in Wiss. Abhandlungen, Vol. II, reprint 42, p. 164-223, Barth, Leipzig, 1909.* Entropy, 2015. **17**(4): p. 1971-2009.

11.   Wolfe, C.M., N. Holonyak, and G.E. Stillman, *Physical properties of semiconductors*. 1989: Prentice Hall.

12.   Hall, E.H., *On a New Action of the Magnet on Electric Currents.* American Journal of Mathematics 1879. **2**: p. 287-292.

13.   van der PAUYV, L., *A method of measuring specific resistivity and Hall effect of discs of arbitrary shape.* Philips Res. Rep., 1958. **13**: p. 1-9.

14. *Voltage Generation by Rotating an Arbitrary-Shaped Metal Loop around Arbitrary Axis in the Presence of an Axial Current Distribution.* Journal of Electromagnetic Analysis and Applications, 2010. **02**(06): p. 395.

15. Giuliani, G., *Vector potential, electromagnetic induction and 'physical meaning'.* European Journal of Physics, 2010. **31**(4): p. 871.

16. Jervis, T.R. and E.F. Johnson, *Geometrical magnetoresistance and hall mobility in gunn effect devices.* Solid-State Electronics, 1970. **13**(2): p. 181-189.

17. Baker, D.R. and J.P. Heremans, *Linear geometrical magnetoresistance effect: Influence of geometry and material composition.* Physical Review B, 1999. **59**(21): p. 13927-13942.

18. Donetti, L., F. Gamiz, and S. Cristoloveanu, *Monte Carlo simulation of Hall and magnetoresistance mobility in SOI devices.* Solid-State Electronics, 2007. **51**(9): p. 1216-1220.

19. Ng, G., D. Vasileska, and D.K. Schroder, *Calculation of the electron Hall mobility and Hall scattering factor in 6H-SiC.* Journal of Applied Physics, 2009. **106**(5): p. 053719.

20. Chang, S.-J., M. Bawedin, and S. Cristoloveanu, *Mobility investigation by geometrical magnetoresistance in fully depleted MOSFETs and FinFETs.* Electron Devices, IEEE Transactions on, 2014. **61**(6): p. 1979-1986.

21. Newman, N., et al., *Electrical study of Schottky barriers on atomically clean GaAs (110) surfaces.* Physical Review B, 1986. **33**(2): p. 1146.

22. Kawabata, A., *Theory of negative magnetoresistance I. Application to heavily doped semiconductors.* Journal of the Physical Society of Japan, 1980. **49**(2): p. 628-637.

23. Kawaguchi, Y. and S. Kawaji, *NEGATIVE MAGNETORESISTANCE IN SILICON(100) MOS INVERSION-LAYERS.* Journal of the Physical Society of Japan, 1980. **48**(2): p. 699-700.

24. Kawaguchi, Y., H. Kitahara, and S. Kawaji, *NEGATIVE MAGNETORESISTANCE IN A 2-DIMENSIONAL IMPURITY BAND IN CESIATED P-SI(111) SURFACE INVERSION LAYERS.* Surface Science, 1978. **73**(1): p. 520-527.

25. Kawaguchi, Y., H. Kitahara, and S. Kawaji, *ANGULAR DEPENDENT NEGATIVE MAGNETORESISTANCE IN SI-MOS (111) INVERSION LAYERS.* Solid State Communications, 1978. **26**(11): p. 701-703.

26. Blood, P. and R. Tree, *The scattering factor for geometrical magnetoresistance in GaAs.* Journal of Physics D: Applied Physics, 1971. **4**(9): p. L29.

27. Altermatt, P.P., et al., *Specifying targets of future research in photovoltaic devices containing pyrite (FeS 2) by numerical modelling.* Solar energy materials and solar cells, 2002. **71**(2): p. 181-195.

APPENDIX

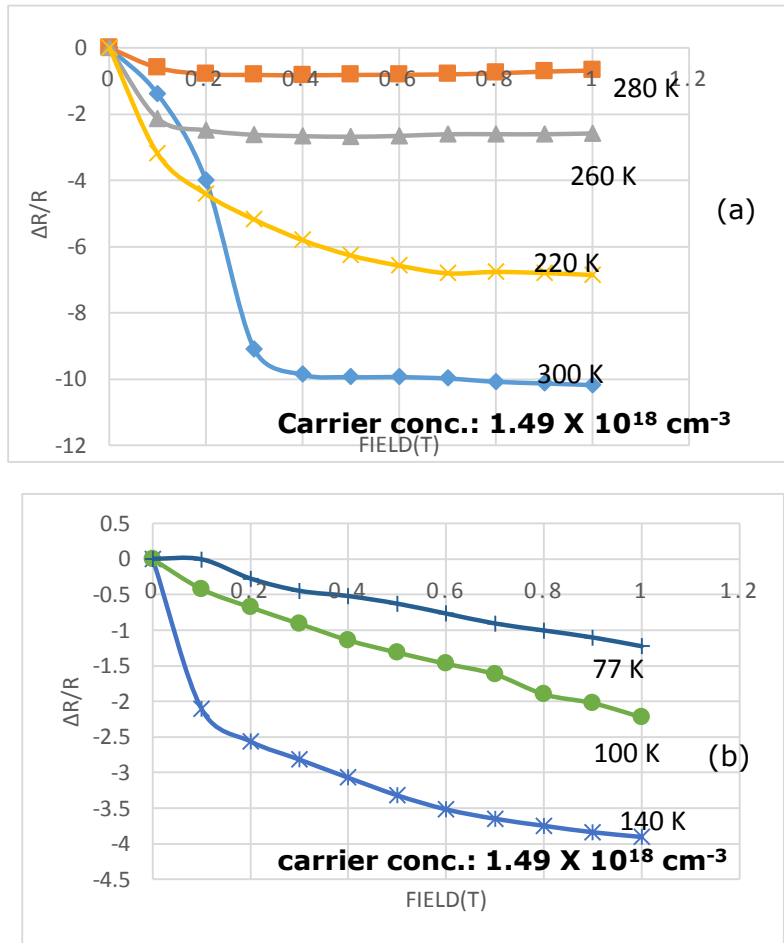NEGATIVE MAGNETORESISTANCE OBSERVED IN HIGHER DOPED GaAs SAMPLE

Figure 38: Magnetoresistance results Field versus ΔR/R in GaAs with carrier concentration of 2.1 x 10^{18} cm^{-3} sample over temperature ranges (a) 300 K- 220 K, (b) 140 K- 77 K